processes

MDPI

Article

The Assessment of Anticancer and VEGFR-2 Inhibitory Activities of a New 1*H*-Indole Derivative: In Silico and In Vitro Approaches

Eslam B. Elkaeed [1], Reda G. Yousef [2], Hazem Elkady [2], Ibraheem M. M. Gobaara [3], Aisha A. Alsfouk [4], Dalal Z. Husein [5], Ibrahim M. Ibrahim [6], Ahmed M. Metwaly [7,8,*] and Ibrahim H. Eissa [2,*]

1 Department of Pharmaceutical Sciences, College of Pharmacy, AlMaarefa University, Riyadh 13713, Saudi Arabia; ikaeed@mcst.edu.sa
2 Pharmaceutical Medicinal Chemistry & Drug Design Department, Faculty of Pharmacy (Boys), Al-Azhar University, Cairo 11884, Egypt; redayousof@azhar.edu.eg (R.G.Y.); hazemelkady@azhar.edu.eg (H.E.)
3 Zoology Department, Faculty of Science (Boys), Al-Azhar University, Cairo 11884, Egypt; ibraheemgobaara@azhar.edu.eg
4 Department of Pharmaceutical Sciences, College of Pharmacy, Princess Nourah Bint Abdulrahman University, P.O. Box 84428, Riyadh 11671, Saudi Arabia; aaalsfouk@pnu.edu.sa
5 Chemistry Department, Faculty of Science, New Valley University, El-Kharja 72511, Egypt; dalal_husein@sci.nvu.edu.eg
6 Biophysics Department, Faculty of Science, Cairo University, Cairo 12613, Egypt; iabdelmagid@sci.cu.edu.eg
7 Pharmacognosy and Medicinal Plants Department, Faculty of Pharmacy (Boys), Al-Azhar University, Cairo 11884, Egypt
8 Biopharmaceutical Products Research Department, Genetic Engineering and Biotechnology Research Institute, City of Scientific Research and Technological Applications (SRTA-City), Alexandria 21934, Egypt
* Correspondence: ametwaly@azhar.edu.eg (A.M.M.); ibrahimeissa@azhar.edu.eg (I.H.E.)

Abstract: Corresponding to the reported features of anti-VEGFR-2-approved compounds, a new 1*H*-indole derivative (compound **7**) was designed. The inhibitory potential of the designed compound was revealed via a molecular docking study that showed the appropriate binding. Then, MD simulation (six studies) over a period of 100 ns was performed to confirm the precise binding and optimum energy. Additionally, MM-GBSA reaffirmed the perfect binding, exhibiting a total precise energy of −40.38 Kcal/Mol. The MM-GBSA experiments named the essential amino acids in the protein–ligand interaction, employing the binding energy decomposition and revealing the diversity of interactions of compound **7** inside the VEGFR-2 enzyme. As compound **7** is new, DFT experiments were utilized for molecular structure optimization. Additionally, the DFT results validated the coherent interaction of compound **7** with the VEGFR-2 enzyme. A good value of drug-likeness of compound **7** was acknowledged via in silico ADMET studies. Interestingly, the experimental in vitro prohibitory potential of compound **7** was better than that of sorafenib, demonstrating an IC_{50} value of 25 nM. Notably, the strong inhibitory effects of compound **10** against two cancer cell lines (MCF-7 and HCT 116) were established with IC_{50} values of 12.93 and 11.52 µM, disclosing high selectivity indexes of 6.7 and 7.5, respectively.

Keywords: 1*H*-indole; VEGFR-2 inhibitors; molecular docking; MD simulations; MM-GBSA; PLIP; DFT; ADMET; in vitro antiproliferative

check for updates

Citation: Elkaeed, E.B.; Yousef, R.G.; Elkady, H.; Gobaara, I.M.M.; Alsfouk, A.A.; Husein, D.Z.; Ibrahim, I.M.; Metwaly, A.M.; Eissa, I.H. The Assessment of Anticancer and VEGFR-2 Inhibitory Activities of a New 1*H*-Indole Derivative: In Silico and In Vitro Approaches. *Processes* **2022**, *10*, 1391. https://doi.org/10.3390/pr10071391

Academic Editors: Iliyan Ivanov and Stanimir Manolov

Received: 4 July 2022
Accepted: 14 July 2022
Published: 17 July 2022

Publisher's Note: MDPI stays neutral with regard to jurisdictional claims in published maps and institutional affiliations.

1. Introduction

The WHO has estimated that cancer will become the main cause of death over the upcoming years. Additionally, they have pointed to the dominance of breast cancer (according to the discovery of new cancer cases) in 2020, with more than 2.2 million new cases [1]. Correspondingly, cancer therapy, especially breast cancer, is a challenging area for medicinal chemists to develop treatments that inhibit the growth of cancer cells by

interacting with specific molecular targets and subsequently killing them. Tumor growth and reproduction are associated with increased vascularity (angiogenesis) in cancer cells [2]. Accordingly, anti-angiogenesis mechanisms were considered as one of the potential ways to combat cancer [3]. The vascular endothelial growth factor (VEGF) pathway plays an important role in the incidence of angiogenesis [4]. The vascular endothelial growth factor receptors (VEGFRs) can be divided into three subtypes; VEGFR-1, VEGFR-2, and VEGFR-3. Among the most valuable targets in cancer management, VEGFR-2 is a transmembrane tyrosine kinase receptor that is correlated with cell proliferation, division, motility, adhesion, and angiogenesis [5]. Thus, blocking the VEGFR-2 signaling cascade inhibits cancer cell proliferation [6]. The fact that cancer cells express VEGFR-2 receptors more than normal cells has enabled scientists to create safe and selective drugs to combat angiogenesis in tumor cells without affecting normal cells [7].

Using computers, computational (in silico) chemistry is a scientific approach that applies theoretical and mathematical basics to address and solve chemical problems. Computational chemistry is widely used in the pharmaceutical industry for investigating interactions between potential drugs and biomolecular targets [8]. Our team have synthesized and examined various compounds that were designed as anti-VEGFR-2, belonging to different classes such as quinazoline [9–12], nicotinamides [13], benzoxazole [14], pyridine [15] dihydroquinolones [16], thiourea-azetidine [17,18], and quinoxaline-2 (1*H*)-one [19–23], in addition to thieno [2,3-*d*]pyrimidine [24]. Furthermore, our team utilized the basics of in silico chemistry as a successful tool in molecular design and docking [25,26], structural similarity [27], toxicity [28], ADMET [29], DFT [30,31], MD [32], and pharmacophore [33] investigation.

We herein employ our former experiences in both of in silico chemistry and drug discovery to introduce an effective and selective chemotherapeutic 1*H*-indole derivative focusing on VEGFR-2.

Rationale

Figure 1 demonstrates some reported and FDA-approved VEGFR-2 inhibitors such as sorafenib **I** [34], sunitinib **II** [35], vorolanib **III** [36], nintedanib **IV** [37], and toceranib **V** [38]. These drugs have four key pharmacophoric features that must exist in any inhibitor to fit with the VEGFR-2 active site. The four key features are aromatic ring, spacer moiety, pharmacophore moiety (comprising hydrogen bond donor and hydrogen bond acceptor atoms), and hydrophobic group [20,39,40].

Regarding sunitinib **II**, vorolanib **III**, nintedanib **IV**, and toceranib **V,** these drugs possess 1*H*-indole derivatives as hetero aromatic structures that can occupy the hinge region of the VEGFR-2 active site. In all compounds, it was noticed that the 1*H*-indole derivatives share three characteristics. (i) The NH group at the 1-position was kept free without any substitution. (ii) Except nintedanib **IV**, the 5-position was substituted with the hydrophobic (fluoro) group. (iii) The 1*H*-indole moiety was attached to the rest of the structures at the 3-position. Moreover, sunitinib **II**, vorolanib **III**, nintedanib **IV**, and toceranib **V** have an amide moiety as a pharmacophore that binds the DFG motif region and forms essential hydrogen bonds with Asp1044 and Glu833.

Taking these characteristics into consideration, we designed a modified analog that kept the main characteristics of the lead compounds (**II**–**V**). As appeared in Figure 2, the designed molecule has a 1*H*-indole moiety as a hetero aromatic structure that can occupy the hinge region of the VEGFR-2 active site. The 1*H*-indole moiety has a free NH group with a substitution at the 5-position with a hydrophobic methoxy group. In addition, the 1*H*-indole moiety was attached to the rest of the structures at the 3-position as in the lead compounds. Furthermore, the designed molecule has an amide moiety as a pharmacophore that binds the DFG motif region at the VEGFR-2 active site. The linker structure of the designed compound consisted of an *N*′-methylene benzohydrazide moiety that can form hydrophobic and hydrophilic interactions at the gatekeeper region. Finally, a plain phenyl ring was utilized as a hydrophobic tail in the designed molecule to form a hydrophobic interaction at the allosteric binding pocket.

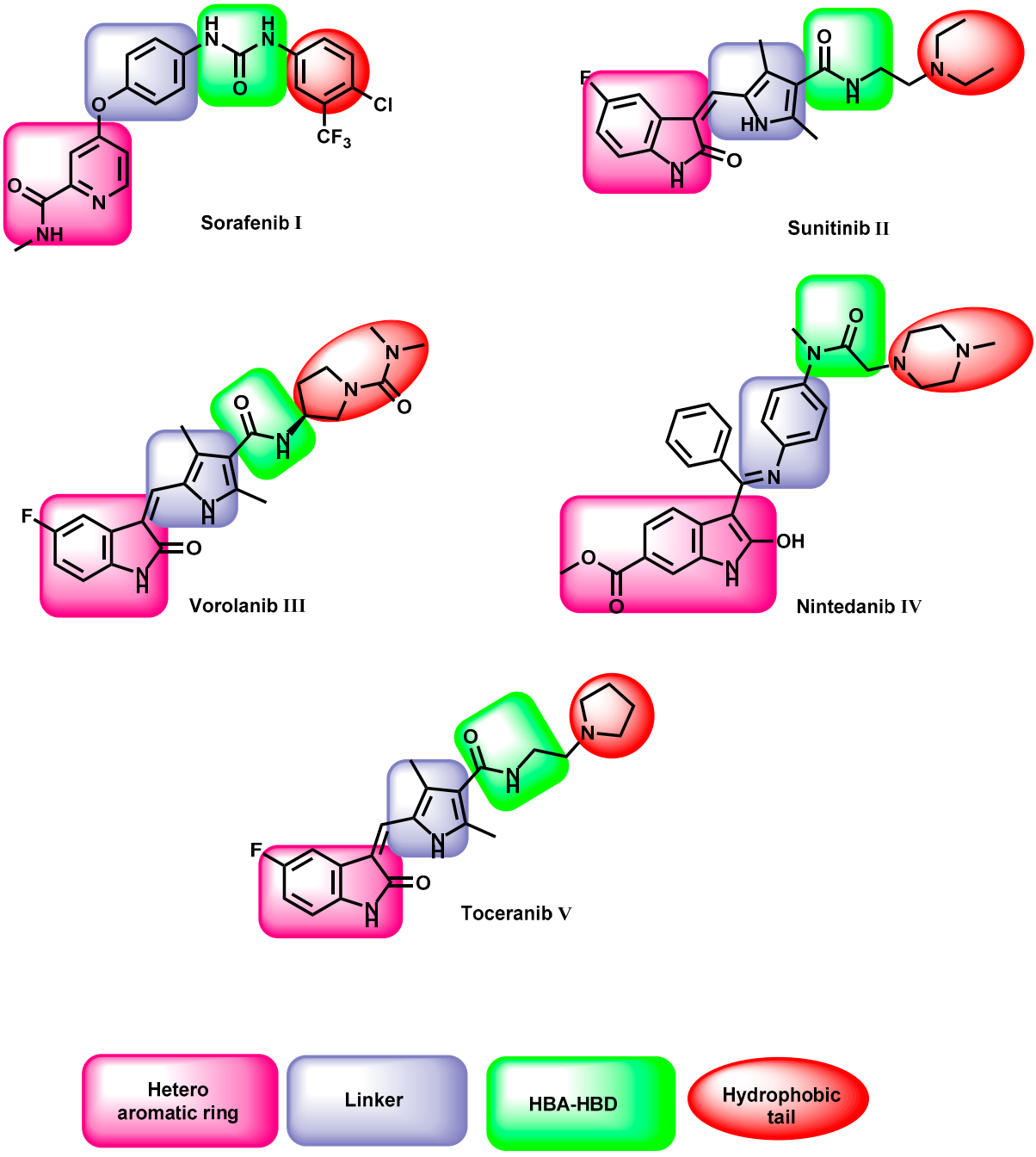

Figure 1. Sorafenib and some FDA-approved 1*H*-indole derivatives working as VEGFR-2 inhibitors show the essential pharmacophoric features.

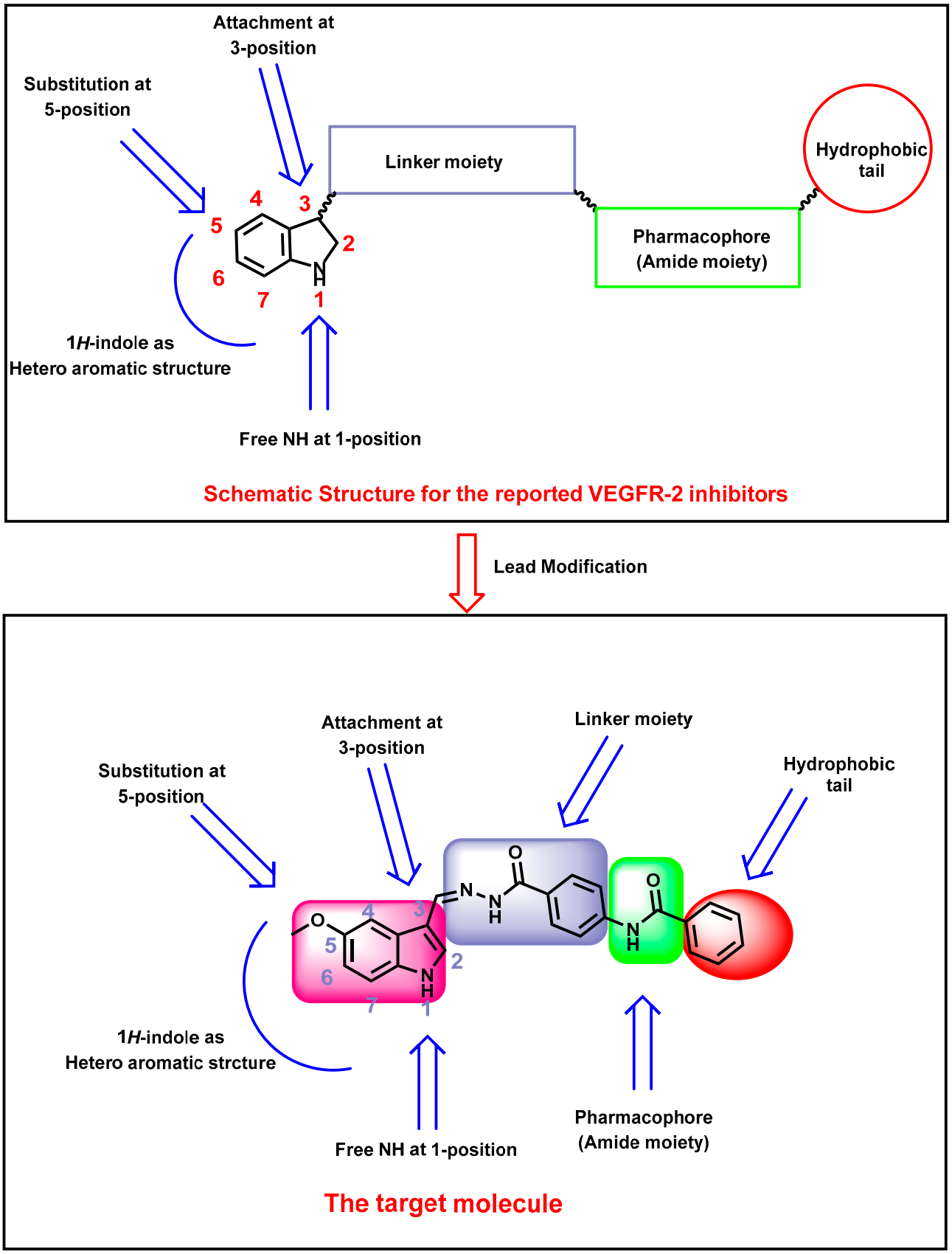

Figure 2. The design rationale of the targeted compound.

2. Results and Discussion

2.1. In Silico Studies

2.1.1. Docking Study

Molecular docking has been applied as an essential tool in the process of drug design and discovery for various bioactive compounds [39,40], including antispasmodics [41], antimicrobials [42], and antimalarials [43]. Compound **7** was docked into the VEGFR-2 ATP binding site to better understand the pattern by which it bounds to the active site [38–40]. Following the preparation of the downloaded protein (PDB ID: 2OH4, resolution: 2.05 Å), the native co-crystallized inhibitor was re-docked against the catalytic VEGFR-2 site as a validation step for the docking protocol. The validation process successfully formed an RMSD value of 0.79 that indicated the validity of the docking operation (Figure 3).

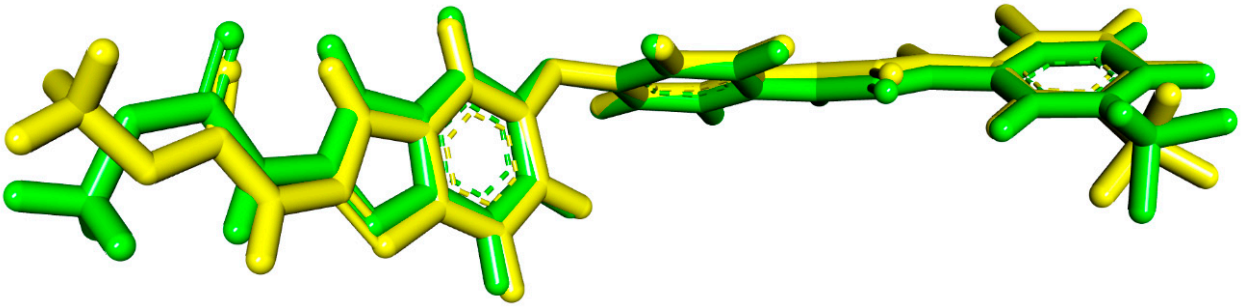

Figure 3. Validation step inside VEGFR-2 catalytic site; native ligand (green) and the obtained pose (yellow).

The surveillance of interaction types between sorafenib and the VEGFR-2 active pocket showed that it could form two main types of interactions (Figure 4). The first type was represented by three H-bonding interactions with the critical amino acids in the VEGFR-2 catalytic site. This includes Cys917 in the hinge region, and Asp1044, and Glu883 in the DFG motif. The second type of interactions comprised a huge network of π interactions between sorafenib and the hydrophobic amino acids (Val846, Val914, Val897, Phe1045, and Cys1043 in the linker region, Leu1033, Leu838, Val846, Phe1045, and Ala864 in the hinge region, and Leu1017, His1024, Ile890, Ile886, and Leu887 in the hydrophobic pocket).

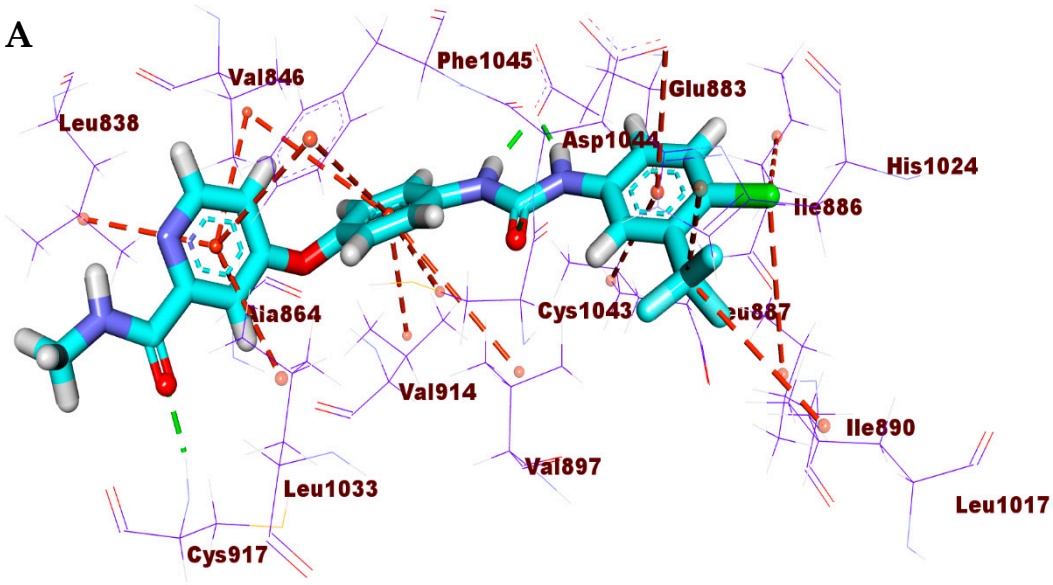

Figure 4. *Cont.*

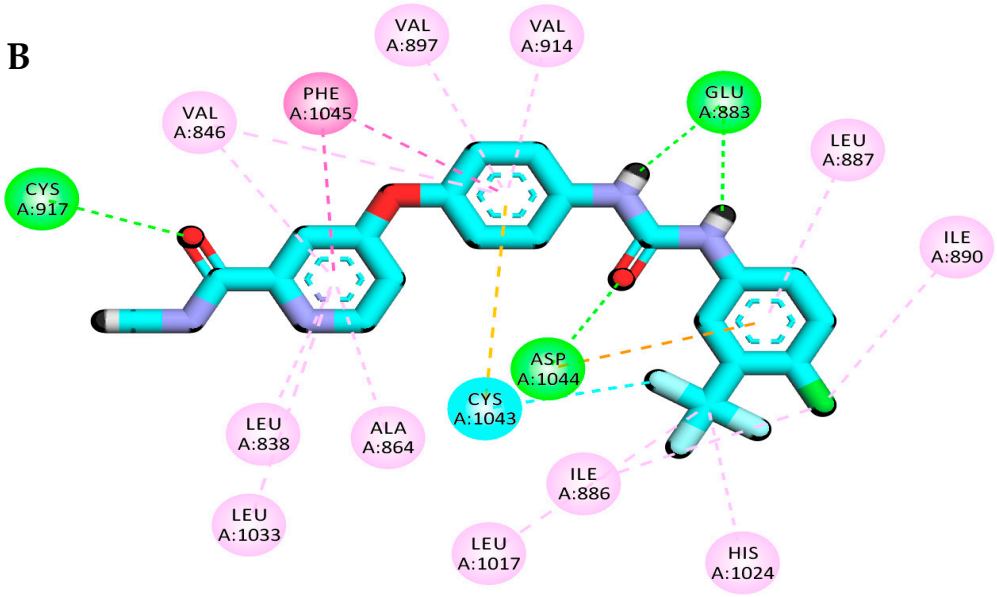

Figure 4. Sorafenib binding pattern, (**A**) 3D and (**B**) 2D.

Docking results for compound **7** revealed strong binding interactions with the VEGFR-2 enzyme, similar to sorafenib. Simply, compound **7** formed a critical hydrogen bond with Cys917 via its indole nitrogen, similar to the pyridine nitrogen of sorafenib. The methoxy group formed a hydrogen bond with Arg1049. Moreover, the amide moiety (inserted between the two phenyl groups) formed two hydrogen-bonding interactions with Glu883 and Asp1044 amino acids, similar to those of sorafenib's urea group. As well, the central phenyl moiety occupied the linker region to form hydrophobic interactions between Val897, and Val914. Similar to the 3-trifluoromethyl-4-chlorophenyl moiety of sorafenib, the hydrophobic allosteric site of the enzyme was occupied with the terminal phenyl group via interactions with Leu887 and Val897. The binding mode of compound **7** is presented in Figure 5.

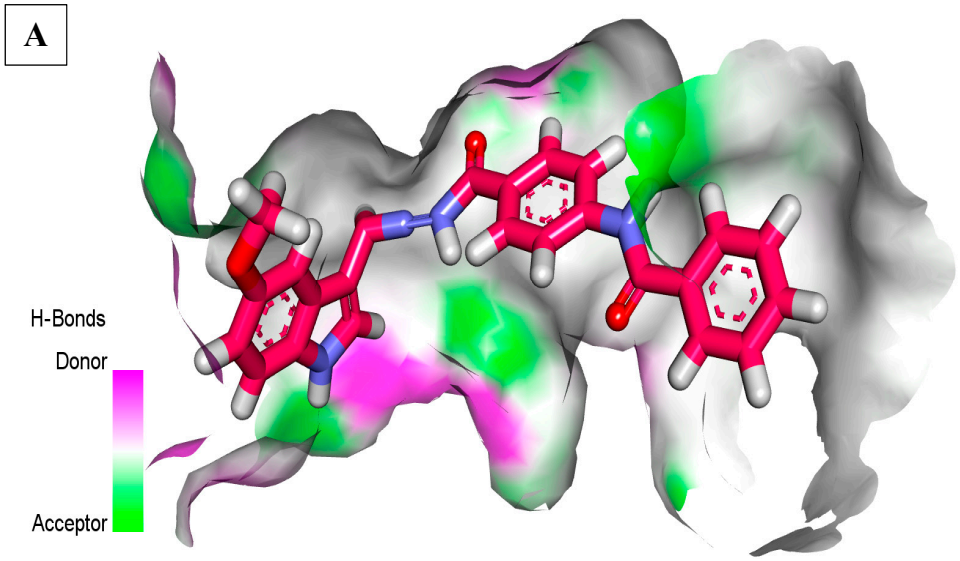

Figure 5. *Cont.*

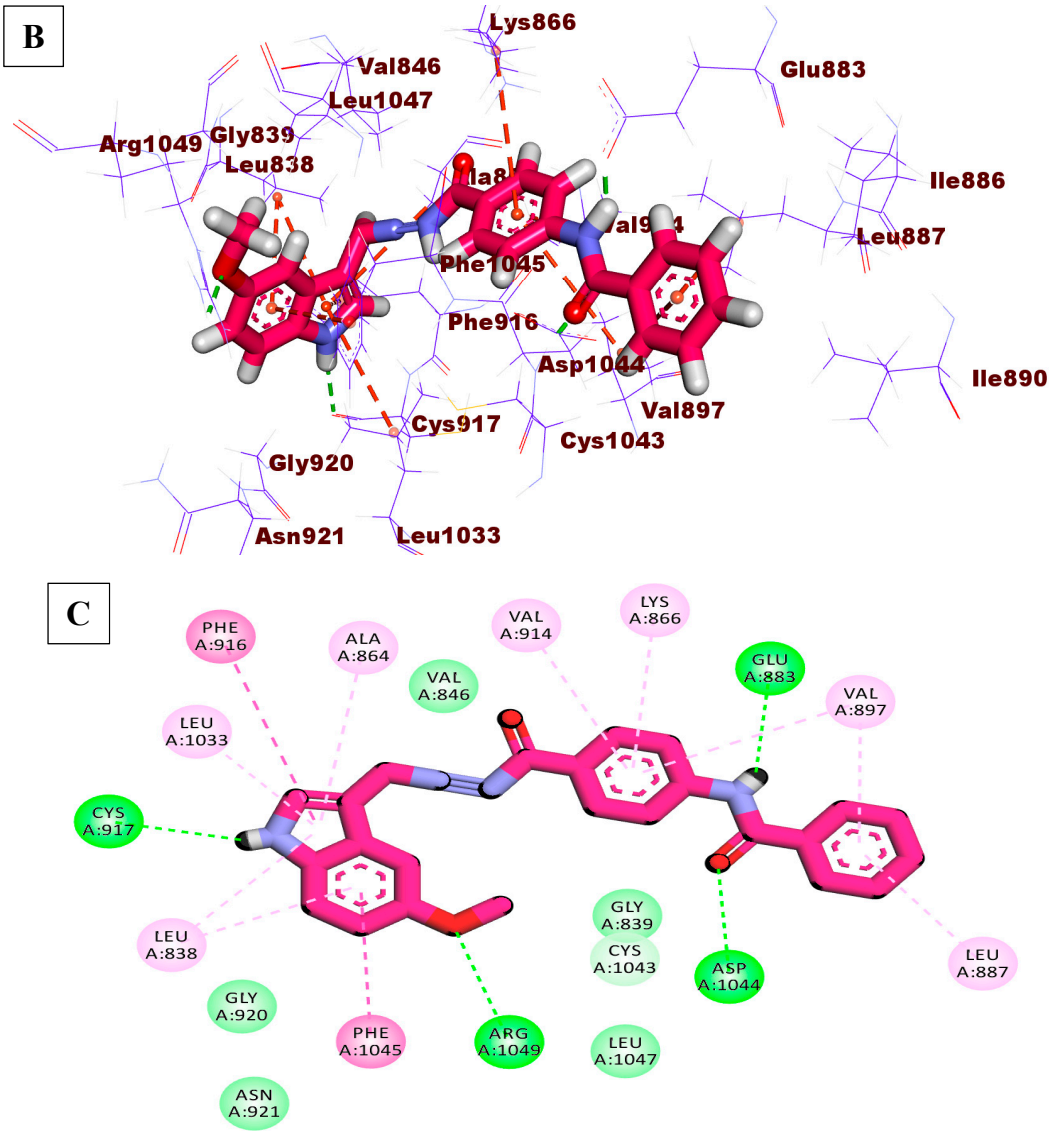

Figure 5. (**A**) Mapping surface, (**B**) 3D, and (**C**) 2D binding pattern of compound **7**.

2.1.2. MD Studies

To study the stability of the compound **7**-VEGFR-2 complex (**7**-VEGFR-2 complex), we performed an MD simulation for the complex. The trajectory was used to extract the RMSD (Figure 6A), RMSF (Figure 6B), SASA (Figure 6C), RoG (Figure 6D), the change in the number of hydrogen bonds (Figure 6E), and the distance between the center of masses between the compound **7** and VEGFR-2 (Figure 6F). The RMSD of the protein and **7**-VEGFR-2 complex shows that the system was changing its conformation in the first half of the simulation before coming to a stable state, with an average of 5 Å and 5.46 Å, respectively. On the other hand, the RMSD of compound **7** shows fluctuations in approximately the first 65 ns, indicating some intrinsic movement of the ligand, before coming to stable values at around 3.2 Å. The reason for the increase in the RMSD after 50 ns is the large motion of the L1047:P1066 loop, as shown in the RMSF values. In addition, the terminals show very large fluctuations, reaching 8 Å. On the other hand, nearly most of the amino acids have fluctuations of less than 2 Å. The values of SASA (average = 17,370 Å^2), RoG (average = 20.66 Å), and the change in the number of hydrogen bonds (average = 70 bonds) show that the VEGFR-2 conformation is stable, with no unfolding or folding occurring. The distance between the center of mass of compound **7** and VEGFR-2 indicates that compound **7** is bound to VEGFR-2 during the simulation, with an average of 8.08 Å.

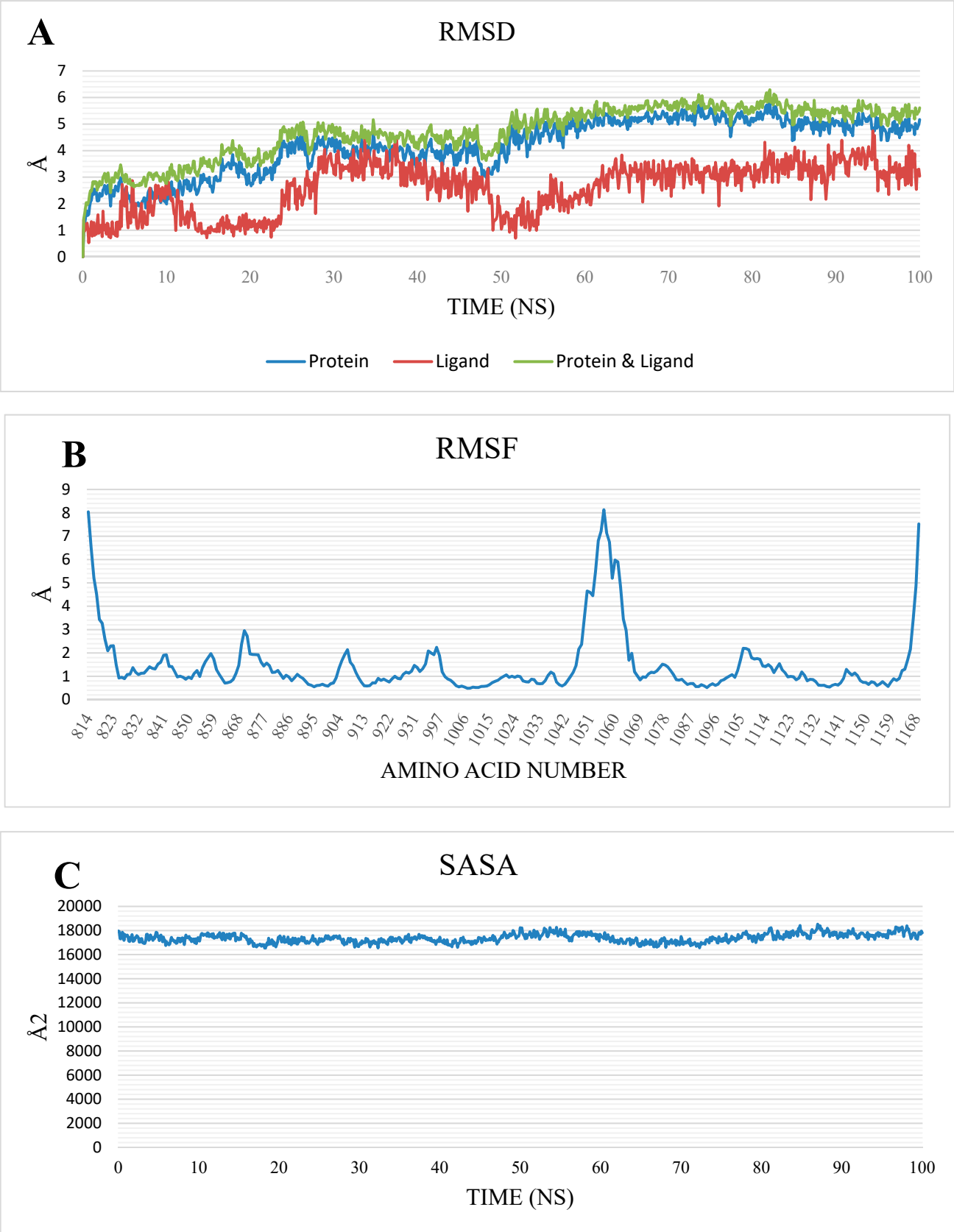

Figure 6. *Cont.*

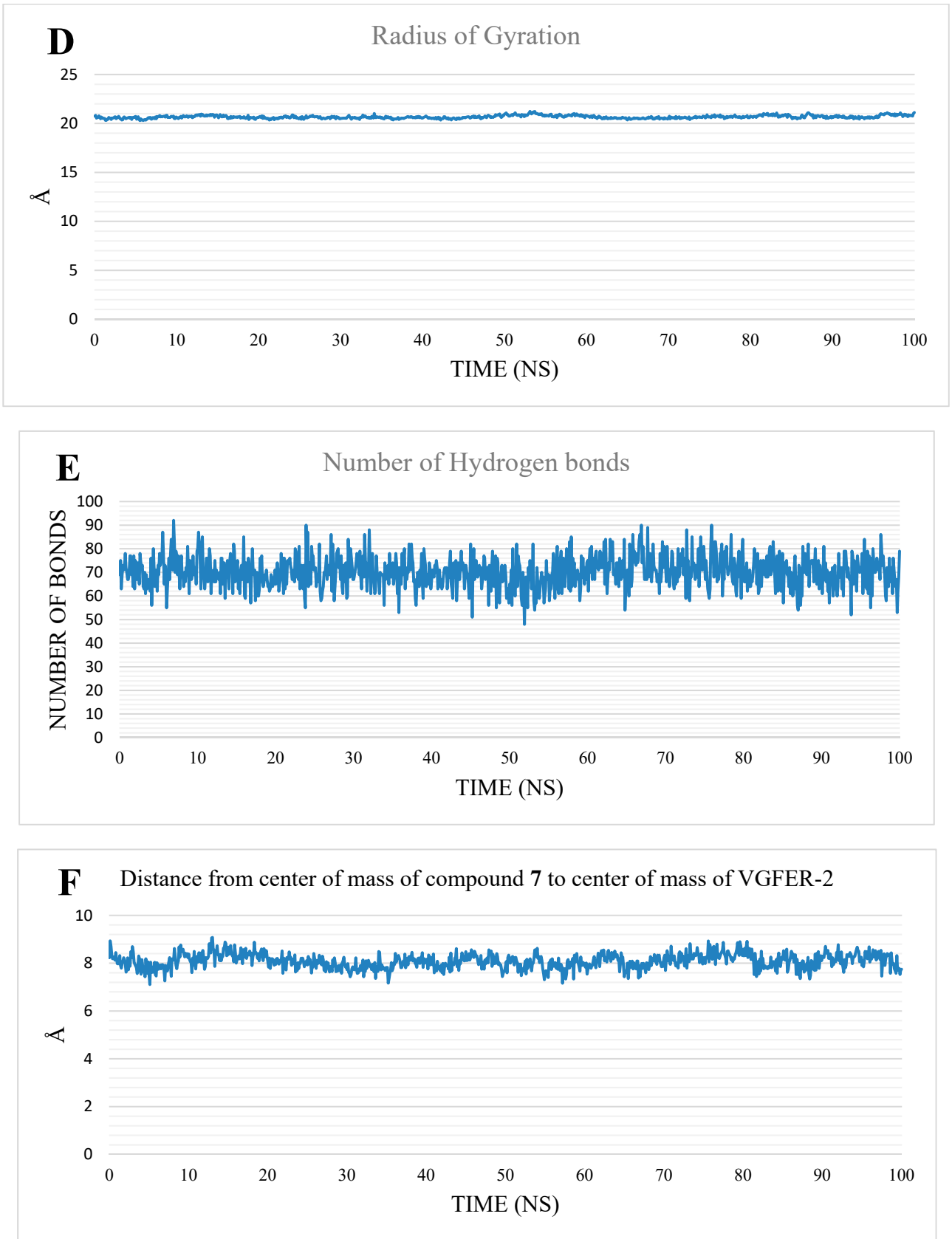

Figure 6. Analyses performed on the trajectory using VMD. (**A**) RMSD values. (**B**) RMSF. (**C**) SASA values. (**D**) RoG. (**E**) Hydrogen bond changes. (**F**) Change in the distance from the center of mass of the **7**-VEGFR-2 complex.

2.1.3. MM-GBSA

To measure the strength of binding, the gmx_MMPBSA library was utilized. Figure 7 shows the values of the energy components of MM-GBSA, and their standard deviations. The binding is mostly due to the van der Waals interaction (an average of −54.8 Kcal/Mol), followed by electrostatic interactions (an average of −25.07 Kcal/Mol) and a total binding energy of −40.38 Kcal/Mol. The amino acid contribution to the binding was measured via the decomposition of MM-GBSA, to know which amino acids are contributing most to the interaction (Figure 8). Eight amino acids showed a contribution to the binding, with values of less than −1 Kcal/Mol. L838, V846, K866, L887, V897, V914, C1043, and F1045 showed binding contributions of −1.07 Kcal/Mol, −1.12 Kcal/Mol, −1.49 Kcal/Mol, −1.37 Kcal/Mol, −1.27 Kcal/Mol, −1.11 Kcal/Mol, −3.21 Kcal/Mol, and −1.80 Kcal/Mol, respectively.

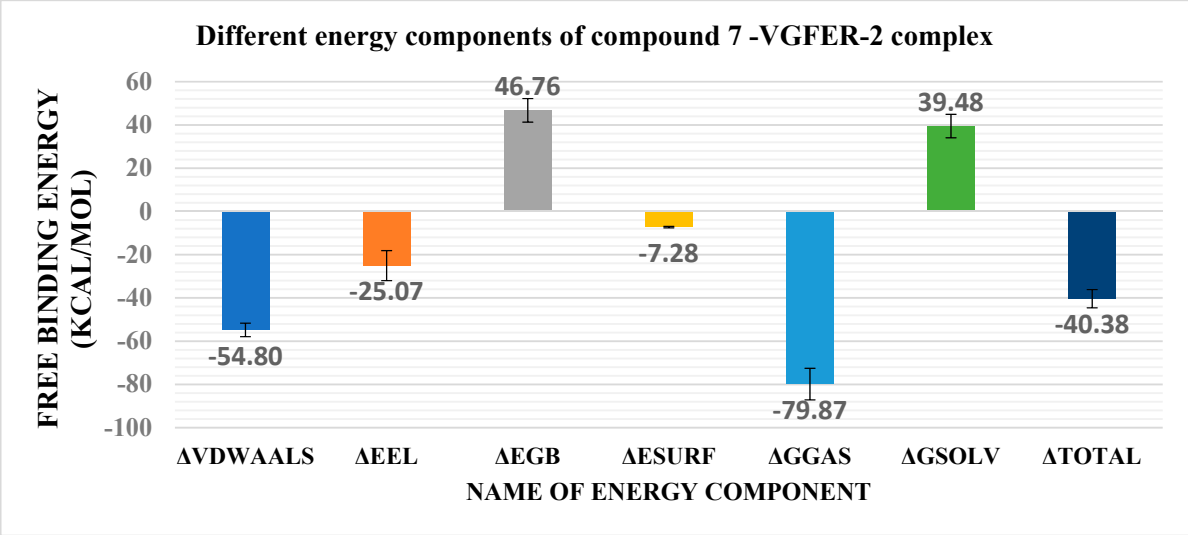

Figure 7. Different energy components obtained from the MM-GBSA analysis. Bars represent the standard deviation values.

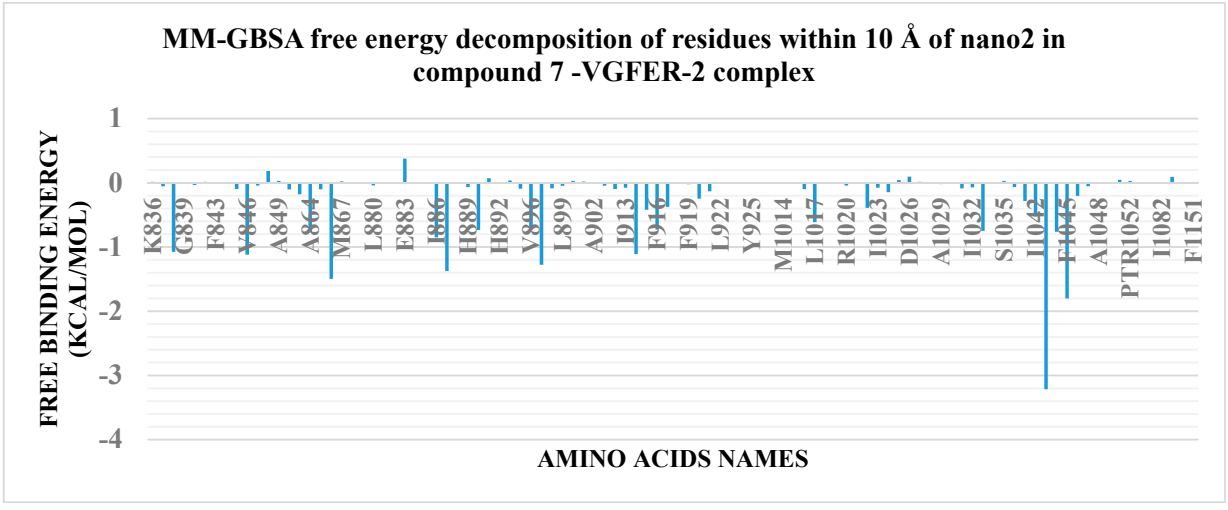

Figure 8. Free binding energy decomposition of amino acids around 10 Å of the **7**-VEGFR-2 complex.

To know the numbers and types of interaction, the trajectory was clustered, and for each cluster, a representative frame was obtained that was used with the PLIP webserver. Table 1 shows the number and types of interactions for each frame. The predominant interaction is the hydrophobic interaction in all of the representative frames that support

the value of the van der Waals component in MM-GBSA analysis. In addition, PLIP outputs the .pse file that shows the 3D interaction pattern for each representative frame (Figure 9).

Table 1. Variation of interactions between compound **7** and VEGFR-2, as obtained from the PLIP webserver for the representative frame of each cluster.

Cluster Number	No. of Hydrogen Bonds	Amino Acids in the Receptor	No. of Hydrophobic Interactions	Amino Acids in the Receptor
C1	3	K866–E915–D1044	6	I886–L887–I890–L1017–L1033–F1045
C2	3	K866–E915–D1044	4	I886–I890–L1017–L1033
C3	3	K866–E915–D1044	7	I886–I890 (2)–F916–L1017–D1044–F1045

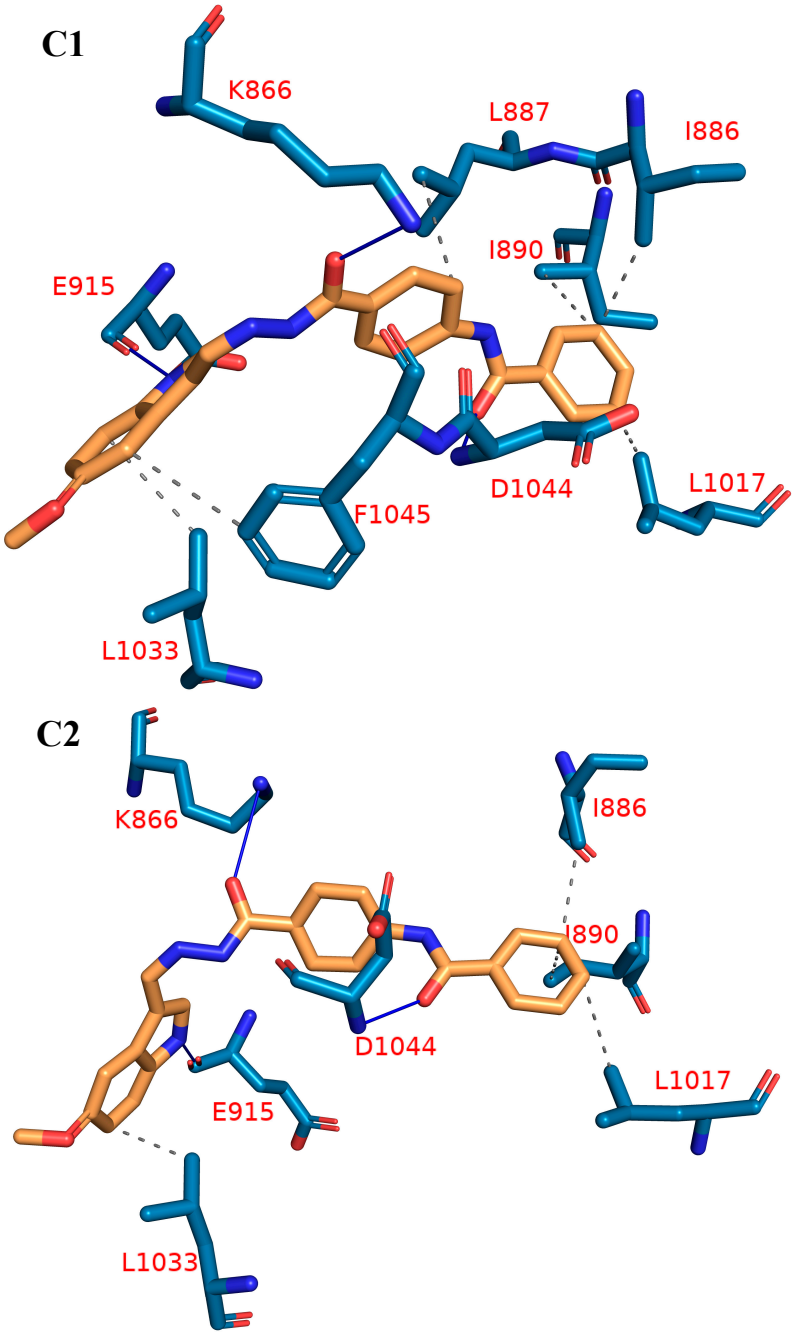

Figure 9. *Cont.*

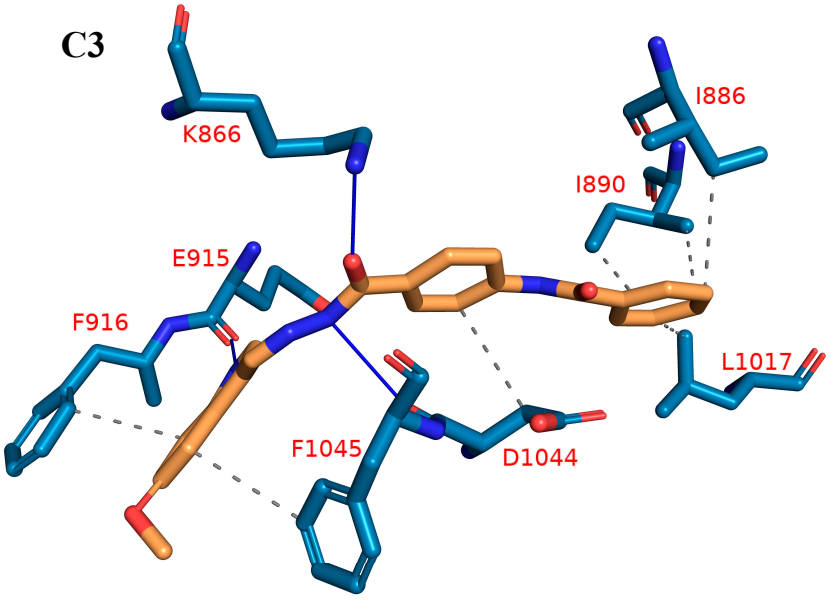

Figure 9. (**C1**–**C3**) Three-dimensional interaction between compound **7**-VEGFR-2 complex in each of the representative frames for each cluster. Amino acids are shown as blue sticks. Compound **7** is shown as orange sticks. Grey dashed lines: hydrophobic interaction. Blue solid lines: hydrogen bonds.

2.1.4. Density Functional Theory (DFT)

Molecular Structure Optimization

The nucleophilic attack of *N*-(4-(hydrazinecarbonyl)phenyl)benzamide to 5-methoxy-1*H*-indole-3-carbaldehyde results in a Schiff base formation through the imine bond (C11-N13). The optimized structure of the formed Schiff base compound is represented in Figure 10. As shown in Figure 10, the imine bond length was found to be 1.28577 Å, while the (C9C11N13) and (C11N13C14) angles were found to be 118.21° and 129.37°, respectively.

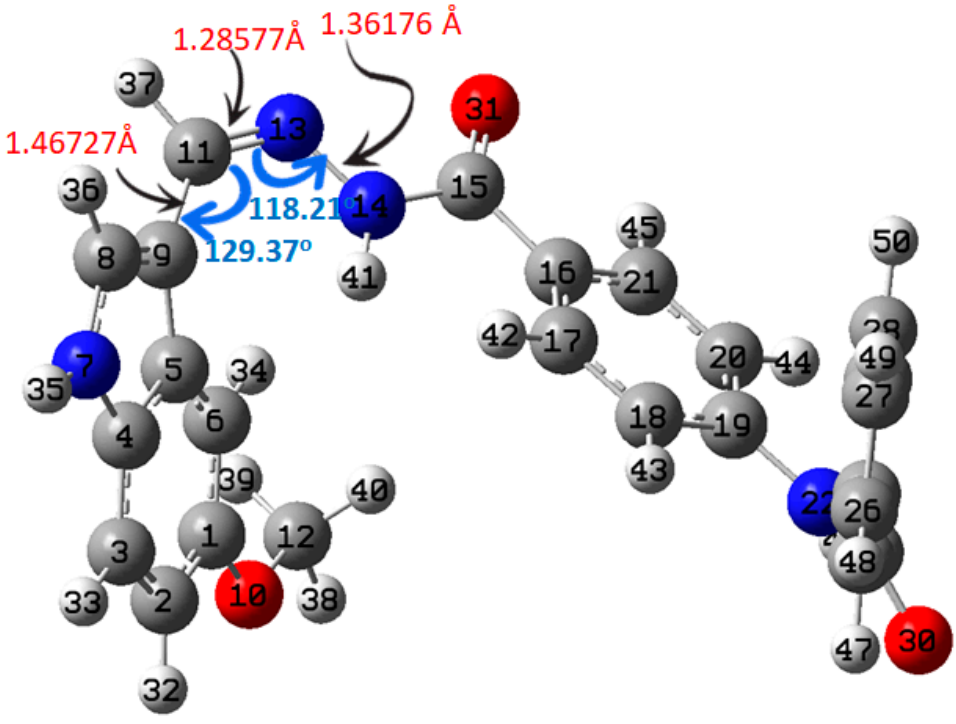

Figure 10. The optimized molecular structure of the selected compound at B3LYB/6-311++G(d,p).

Quantum Chemistry Calculations

The quantum chemistry calculations have been employed as a successful tool in the discovery of active compounds targeting various diseases such as prostate cancer [44], inflammation [45], and malignant glioblastoma [46]. The quantum chemistry calculations were conducted using the Gaussian(R) 09 program at the B3LYP level, together with the 6-311++G(d,p) basis set and the density functional theory (DFT) approach. As depicted in Figure 11, the electronic density of the highest occupied molecular orbital (HOMO) is localized on the heteroaromatic ring system, while in the lowest unoccupied molecular orbital (LUMO), the electronic density is located over the central linker and phenylbenzamide moieties. Frontier molecular orbital (FMO) theory suggested that HOMO serves as a donor, and LUMO serves as an acceptor for electrons. Both HOMO and LUMO have important roles in electronic investigations, and are essential to modern molecular biology and biochemistry when using quantum chemical calculations. A molecule is thought to be softer and more chemically reactive when its energy gap is small. A molecule is assumed to have greater chemical hardness and to be more stable when it has a large energy gap. The FMO gives very significant evidence for the stability, utilizing the difference in the energy (E_{gap}) of the frontier orbitals. Chemical quantum parameters are related to the inhibition efficiency of compound **7**, such as the chemical potential (μ), global hardness (η), maximal charge acceptance (ΔN_{max}), and energy change (ΔE); global softness (σ), electronegativity (χ), electrophilicity index (ω), ionization potential (IP), and electron affinity (EA) were calculated according to the equations of Koopmans' theory (Table 2) (the equations were detailed in Supporting Data).

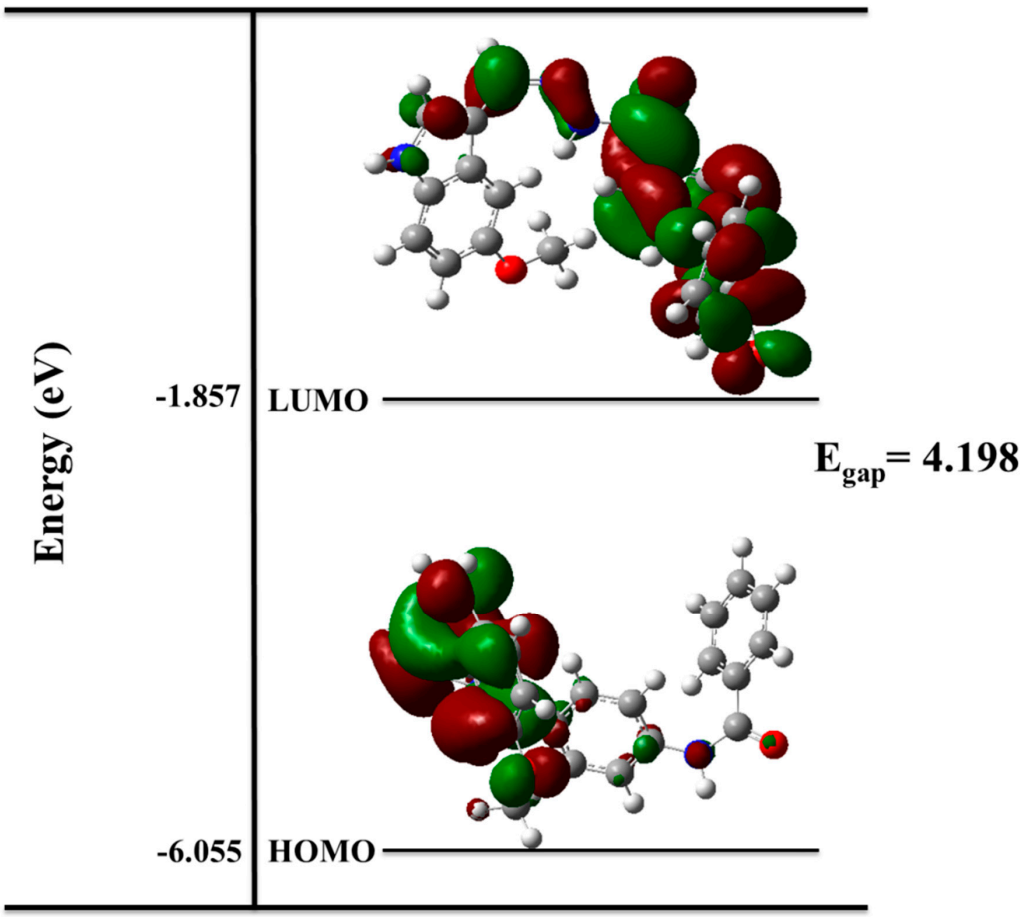

Figure 11. Energy gap (E_{gap}), frontier molecular orbitals; HOMO and LUMO at the ground state at B3LYB/6-311++G(d,p).

Table 2. The DFT calculated global reactivity parameters for comp. **7**.

IP	EA	μ (eV)	χ (eV)	η (eV)	σ (eV)	ω (eV)	Dm (Debye)	TE (eV)	ΔNmax	ΔE (eV)
−6.055	−1.857	−3.956	3.956	2.099	0.476	16.421	6.472	−37,323.8	1.885	−16.421

Global quantum parameters, as well as the dipole moment (Dm) and the total ground state energy (TE), are calculated and summarized in Table 2. The results refer to the ability of comp. **7** to act as an inhibitor against VEGFR-2. For a system in equilibrium, the product of the density of states and probability distribution function gives the number of occupied states per unit volume for a given energy. This number is frequently used to study a variety of physical properties of materials. The total density of state analysis has been calculated and analyzed. The results confirmed the small energy gap of the compound under investigation, as depicted in Figure 12, which confirmed the reactivity of compound **7**. When the E_{gap} of the border orbitals reduces, the inhibitor's efficiency increases [47].

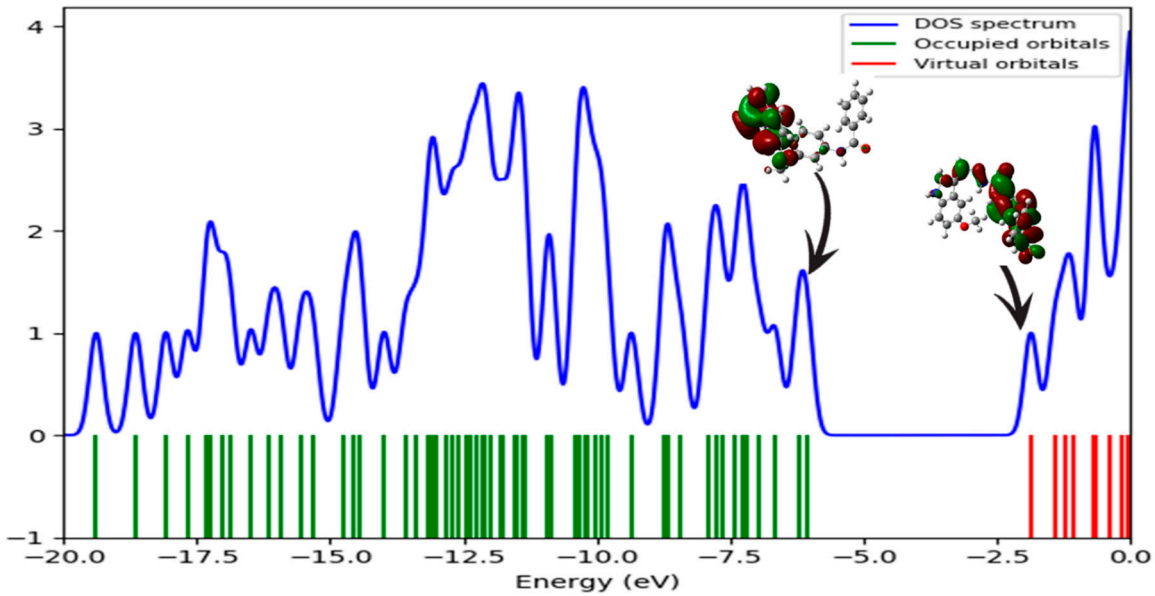

Figure 12. The total density of state analysis for the compound under investigation at B3LYB/6-311++G(d,p).

The Electron Density Maps

The reactivity strength of compound **7** can be predicted using DFT calculations based on the electron density of the donor atoms. The total electron density (TED) map, in Figure 13; represents the whole molecule's electron density. The red regions refer to the high electronegativity chemical sites, which are the O atoms of two carbonyls and methoxy groups in the investigated compound. Such active sites aid with electrophilic attack by amino acids (Cys917 and Glu833). In addition, the yellow-colored regions refer to atoms having a moderate electronegativity and that may form hydrophobic interactions, while the blue zones point to the most favorable positive regions, which accept electrons from the donor atoms of amino acids [48]. The electropositive regions are concentrated over the N-H groups. Such findings explain the nucleophilic attack of amino acids (Cys917 and Glu833) onto the NH groups of the 1*H*-indol and amide moieties, respectively. Furthermore, the possibility of hydrophobic interactions by the 1*H*-indol moiety, the central phenyl group, and the terminal hydrophobic phenyl group was supported by the yellow zones at these functional groups. The electrostatic surface potential (ESP) reveals the inhibition orientation of the molecule on the electrophilic amino acids (Figure 13), which is in the same orientation as the carbonyl and methoxy groups.

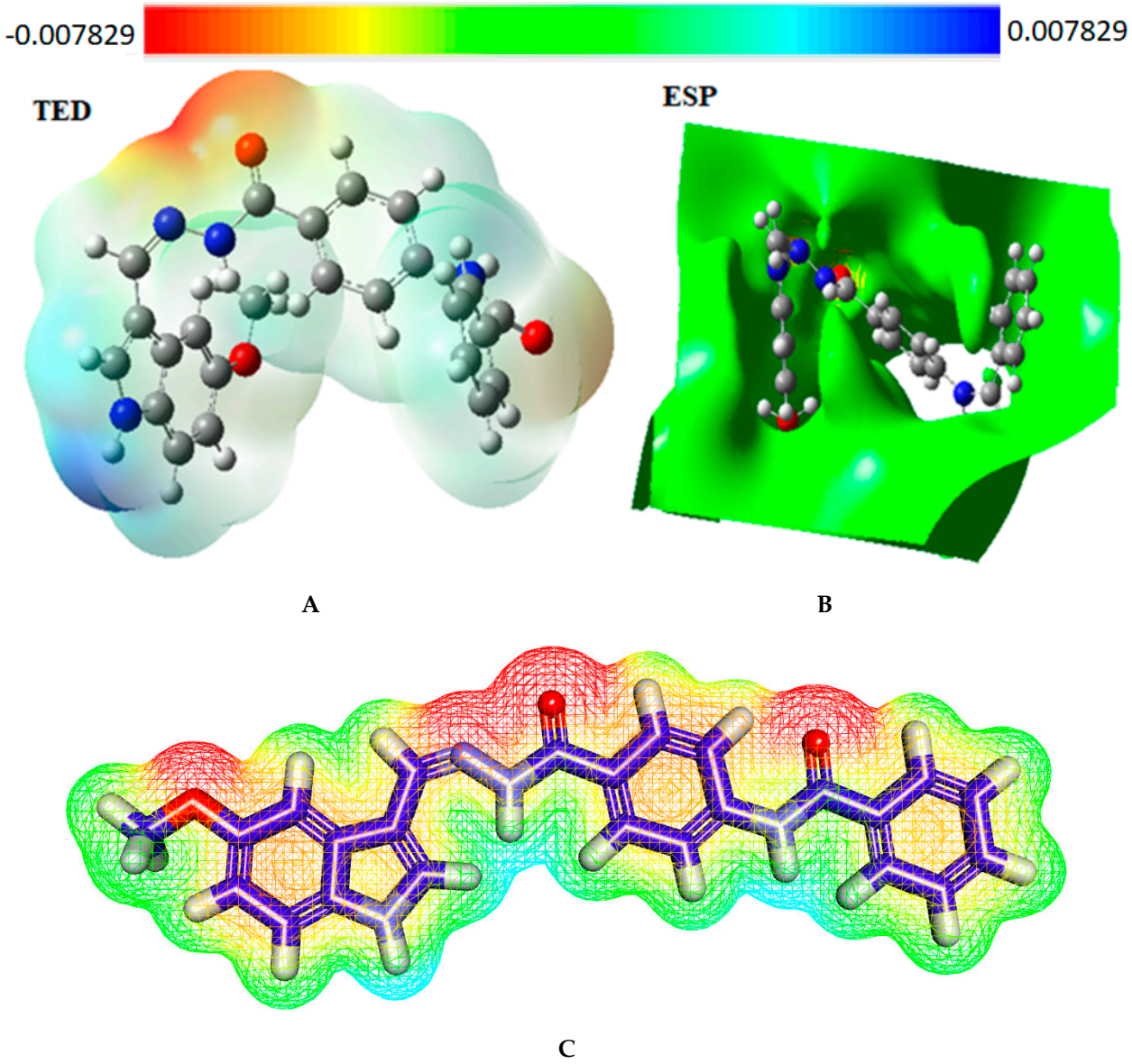

Figure 13. (**A**)**:** Total electron density (TED) and (**B**): electrostatic potential (ESP) maps of the selected compound (Ball and line form) at the 6-311G++(d,p) basis set. (**C**): ESP maps of the compound (stick form).

2.1.5. ADMET Profiling Study

Sorafenib was used as a reference molecule, as the ADMET variables were investigated for compound **7** with Discovery studio 4.0 software. Both compound **7** and sorafenib showed remarkable similarities according to the ADMET results (Figure 14), showing a very low potential to pass the BBB, and good levels of intestinal absorption in addition to low and very low aqueous solubility levels, respectively. Similarly, both molecules presented a non-inhibitory potential against the cytochrome P-450 and CYP2D6, and revealed more than 90% binding percentage with plasma protein.

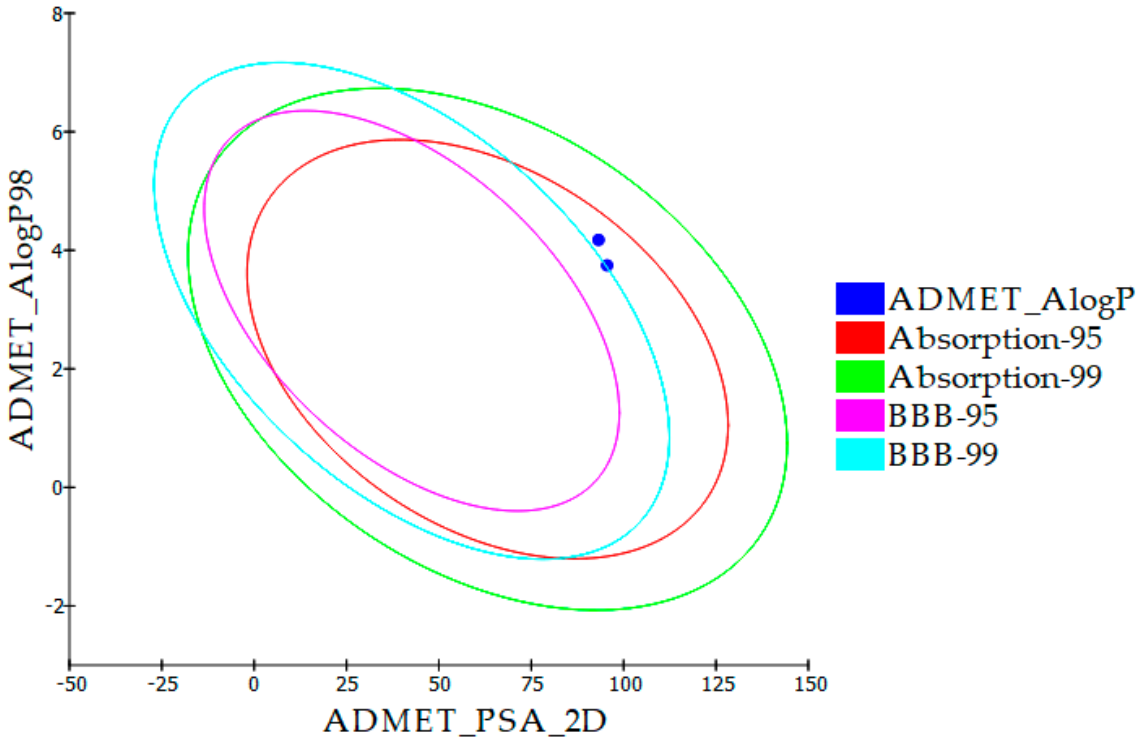

Figure 14. Computational prediction of ADMET parameters for compound **7** and sorafenib.

2.1.6. In Silico Toxicity Studies

In the presented study, five parameters of toxicity were estimated computationally, in accordance with the toxicity models built in the Discovery studio software. The employed models are; the rat-female FDA rodent carcinogenicity (RF-FDA-C) that predicts if the examined compound is carcinogenic or not, carcinogenic potency TD_{50} in a mouse model (TD_{50}-M), maximum tolerated dose in rats (MD-R), rat oral LD_{50} (R-O- LD_{50}), and rat chronic LOAEL (LOAEL-C), in addition to skin and eye irritancy. Table 3 demonstrates the expected general safety of compound **7** against sorafenib.

Table 3. In silico toxicity studies of compound **7** and reference molecule.

Comp.	RF-FDA-C	TD_{50}-M (mg/kg/day)	MD-R (g/kg)	R-O-LD_{50} (g/kg)	LOAEL-C (g/kg)	Skin Irritancy	Eye Irritancy
Compound **7**	Non-Carcinogen	15.480	0.486	0.874	0.136	Non-Irritant	Mild
Sorafenib		19.236	0.089	0.823	0.005	Non-Irritant	Mild

2.1.7. Molecular Similarity

Similarity Check Using Physical Properties

A molecular similarity study using Discovery studio software was conducted to check the structural similarity between the synthesized compound and the FDA-approved 1*H*-inole derivatives (sunitinib **II**, vorolanib **III**, nintedanib **IV**, and toceranib **V**). This technique depends on many molecular properties to assess the structural similarity. These properties include the partition coefficient (ALog p) [49], molecular weight (M. Wt) [50], H-bond donors (HBA) [51], H-bond acceptors (HBD) [52], rotatable bond number [53], number of rings along with aromatic rings and minimum distance [54], as well as the molecular fractional polar surface area (MFPSA) [55]. Table 4 showed the different values for each tested compound, while Figure 15 showed the degree of similarity.

Table 4. Molecular properties of the tested FDA-approved drug and the synthesized compound **7**.

Comp.	ALog p	M. Wt	HBA	HBD	Rotatable Bonds	Rings	Aromatic Rings	MFPSA	Minimum Distance
Toceranib V	2.761	396.458	3	3	5	4	2	0.191	1.12
Compound **7**	3.745	412.441	4	3	6	4	4	0.233	0.00
Sunitinib II	2.997	398.474	3	3	7	3	2	0.179	1.35
Nintedanib IV	4.392	539.625	7	2	8	5	4	0.178	1.83
Vorolanib III	1.671	439.483	3	3	3	4	2	0.213	1.31

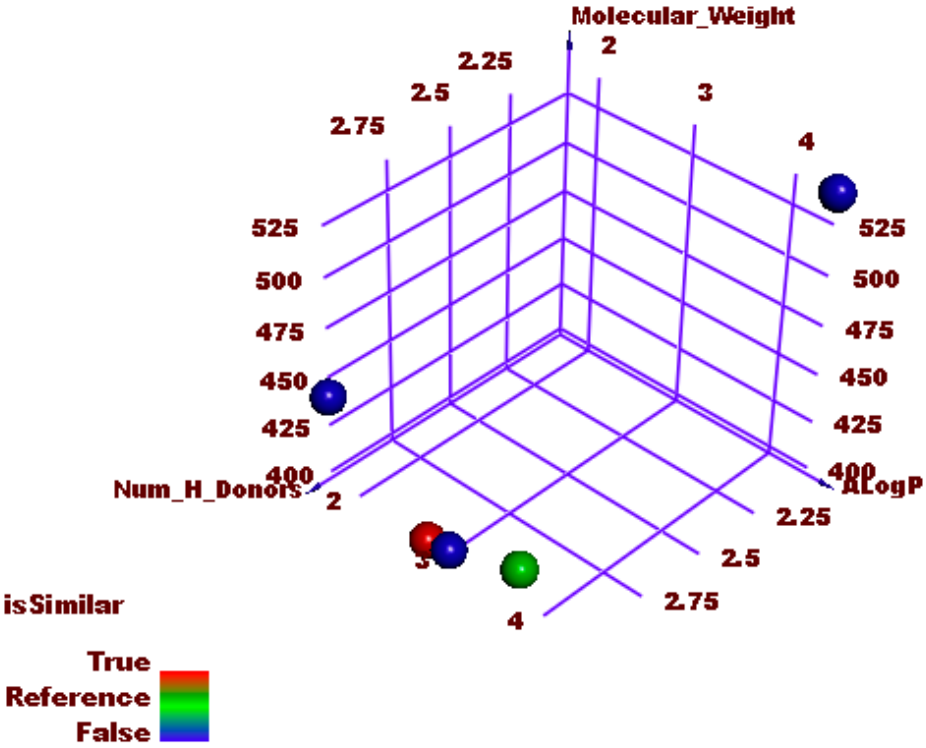

Figure 15. Molecular similarity study between the synthesized compound (green ball) and the FDA-approved 1*H*-inole derivatives (sunitinib, vorolanib, nintedanib, and toceranib). The red ball refers to toceranib (the most similar compound). The blue balls refer to sunitinib, vorolanib, and nintedanib (the less similar drugs).

The results revealed that toceranib **V** has the highest degree of similarity with the synthesized compound **7**.

Flexible Alignment

The 3D flexible alignment was studied for compound **7** and toceranib. The produced figure indicated a high degree of similarity between these compounds. Each feature in the tested compounds takes the same orientation of the corresponding one. In detail, the 5-fluoroindolin-2-one, central phenyl, amide, and terminal phenyl moieties of compound **7** showed the same orientations as 5-methoxyindolin-2-one, 2,4-dimethyl-1H-pyrrole, amide, and 1-ethylpyrrolidine moieties of toceranib, respectively (Figure 16).

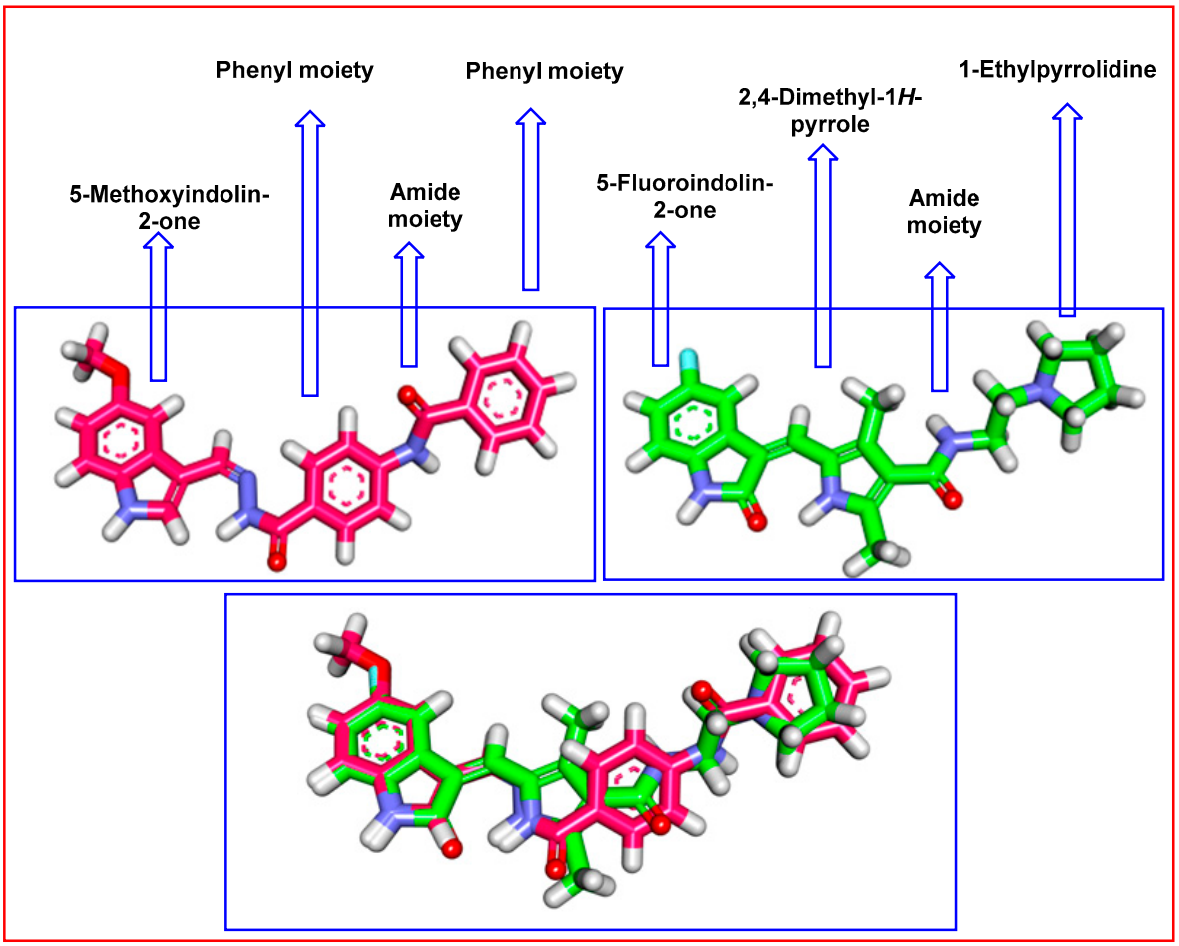

Figure 16. Flexible alignment of compound 8 (green) with sorafenib (pink), showing the same orientation.

2.2. Chemistry

To authenticate the design and the interesting results of the computational studies, the targeted lead compound was synthesized according to Scheme 1. The commercially available material (4-aminobenzoic acid **1**) was first refluxed with methanol and sulfuric acid in accordance with the reported procedure, to afford methyl 4-aminobenzoate **2**. Benzoylation of methyl 4-aminobenzoate **2** was achieved in an ice bath via dropwise addition of benzoyl chloride **3** in DCM in the presence of TEA, to afford compound **4**. Refluxing compound **4** with hydrazine hydrate in ethanol afforded the corresponding acid hydrazide derivative **5**. A mixture of the acid hydrazide derivative **5** and 5-methoxy-1*H*-indole-3-carbaldehyde **6** was refluxed in absolute ethanol and a few drops of glacial acetic acid, to afford the final target compound **7**.

The structure of compound **7** (Figure 17) was validated using spectral analysis. The IR spectrum showed absorption bands at 3287 cm^{-1}, and 1645 cm^{-1} attributed to NH and the amidic carbonyl group, respectively. Moreover, ^{1}H NMR spectra showed singlet signals around δ 11.48 and 10.53 ppm, corresponding to the indole NH and the two amidic NH protons. In addition, an up-field sharp singlet signal corresponding to OCH_3 protons appeared at δ 3.82 ppm. The three protons (6, 7, and 9) of the phenyl ring of the *1H*-indol moiety resonated at δ 7.36 (d, J = 8.8 Hz), 6.88 (dd, J = 8.8, 2.4 Hz), and 7.79 (d, J = 2.4 Hz), respectively. At the same time, proton 2 was presented as a sharp singlet, peaking at δ 8.01. The characteristic proton, 10, resonated clearly as a sharp singlet signal at δ 8.62. Regarding the di para-substituted protons, protons (19, 21) and (18, 22) resonated at δ 7.58 (d, J = 8.2 Hz) and 7.99 (d, J = 8.2 Hz), respectively. Finally, the aromatic protons of

the benzamide moiety resonated at the overlapped areas of 7.68 and 7.96. Matching such findings, the ^{13}C NMR spectra showed characteristic peaks corresponding to the two C=O and OCH_3 groups around δ 166.34, 162.36, and 55.80 ppm, respectively. The carbons (2, 3, 4, 5, 6, 7, 8, and 9) of the phenyl ring of the *1H*-indol moiety resonated at δ (128.3, 112.8, 125.4, 130.4, 112.7, 111.9, 154.8, and 104.6, respectively). The characteristic carbon, 10, resonated at δ 154.2. The di para-substituted carbons (19, 21) and (18, 22) resonated at δ 119.9 and 128.2, respectively. The aromatic carbons (26, 27, 28, 29, 30, and 31) of the benzamide moiety resonated at δ (135.1, 128.2, 128.9, 132.5, 128.9, and 128.2, respectively).

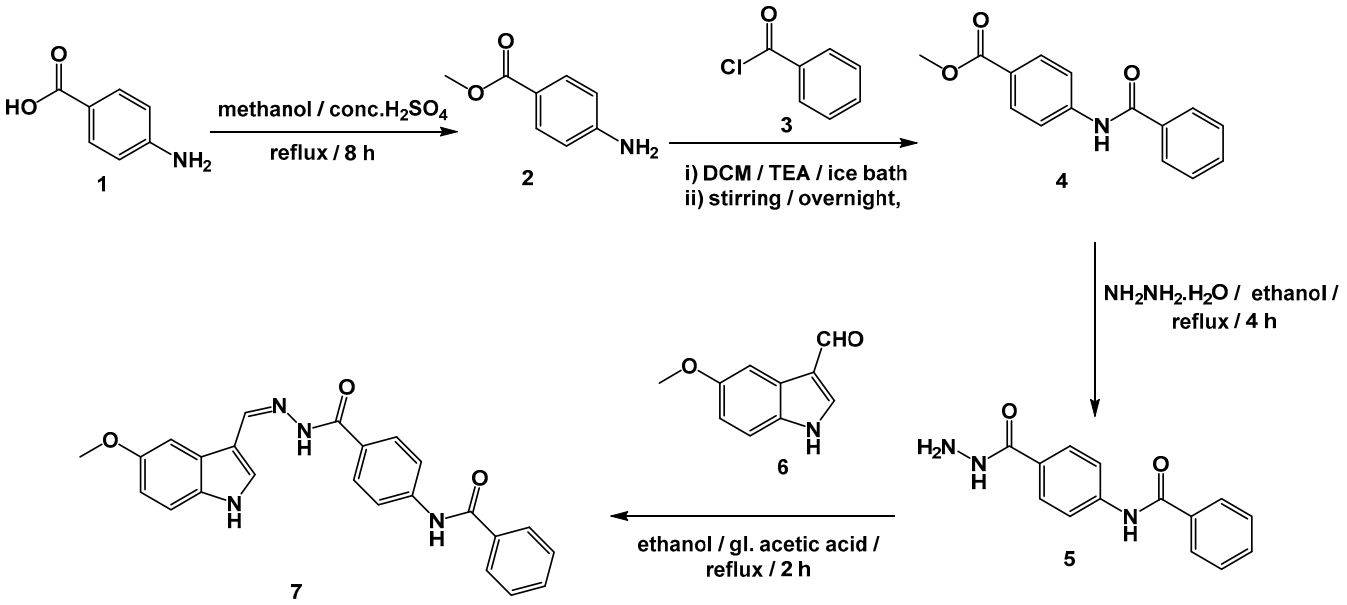

Scheme 1. Synthetic pathway of target compound **7**.

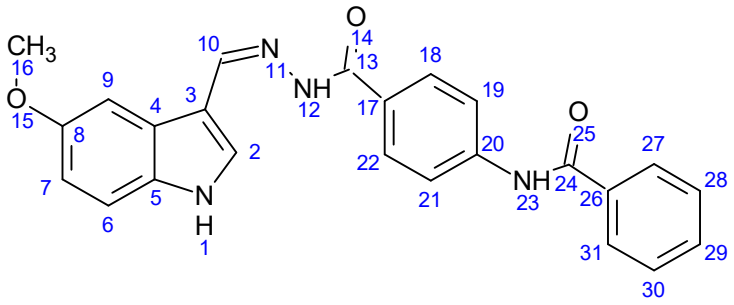

Figure 17. Chemical structure of compound **7**.

2.3. Biological Examinations

2.3.1. VGFER-2 Inhibition

We assessed the in vitro inhibitory potential of compound **7** against VEGFR-2 in comparison to sorafenib, to verify our design, and the several computations conducted that indicated the high affinity of compound **7** for binding to and inhibiting the VEGFR-2 enzyme. Compound **7** showed significant inhibitory activity in vitro (an IC_{50} value of 25 nM) that was lower than that of sorafenib (35 nM). The in vitro results showed that the compound had a great potential to inhibit VEGFR-2, affirming the in silico studies.

2.3.2. Cytotoxicity

To analyze the application of compound **7**'s VEGFR-2 inhibitory potential against cancer, in vitro cytotoxicity studies were conducted using human breast cancer MCF-7, and colon cancer HCT 116 cell lines, with sorafenib as a reference. Table 5 and Figure 18 show

that compound **7** could inhibit the growth of the MCF-7 and HCT 116 cell lines, exhibiting IC_{50} values of 12.93 and 11.52 µM, respectively, in comparison with sorafenib's anticancer potentialities against the same cell lines (4.32 and 7.28 µM, respectively).

Table 5. VGFER-2 inhibition and cytotoxicity of compound **7** and sorafenib.

	MCF-7 IC_{50} (µM)	HCT 116 IC_{50} (µM)	VEGFR IC_{50} (nM)
Compound **7**	12.93 ± 0.54	11.52 ± 0.70	25 ± 1.29
Sorafenib	4.32 ± 0.33	7.28 ± 0.53	35 ± 1.34

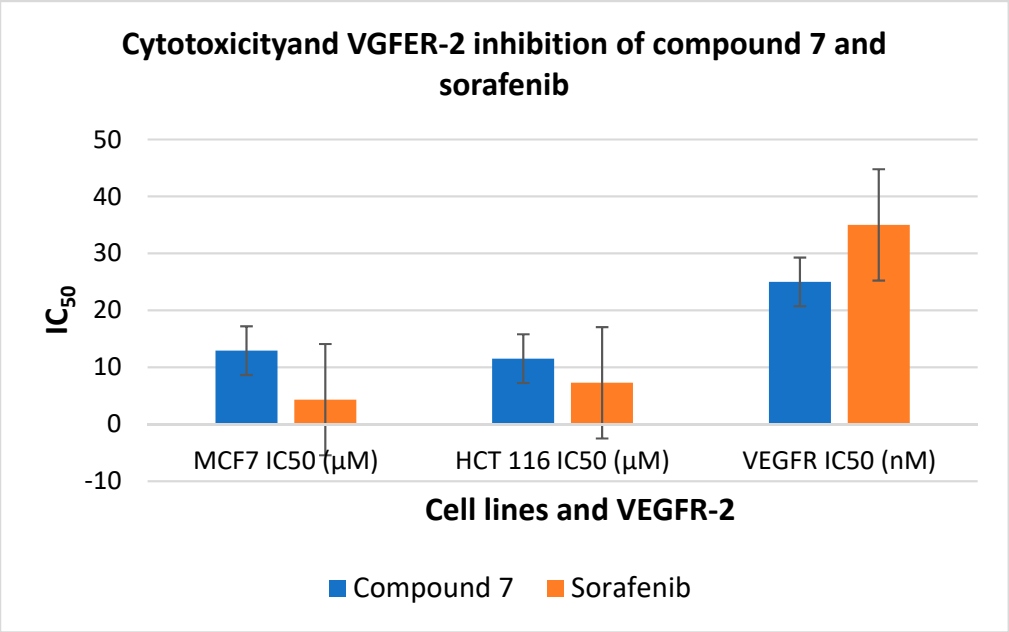

Figure 18. VGFER-2 inhibition and cytotoxicity of compound **7** and sorafenib.

2.3.3. Safety Evaluation

Against normal human cells, W138 cell lines, compound **7** was administered to test its toxicity and to determine its selectivity against cancer cell lines. Notably, compound **7** showed a very high level of safety, manifesting an IC_{50} of 87.26 µM. The obtained selectivity indexes (SI) of compound **7** against MCF-7 and HCT 116 cancer cell lines were very high, at 6.7 and 7.5, respectively.

3. Conclusions

A new 1*H*-indole-derived lead compound has been designed, which keeps the characteristic VEGFR-2 prohibition features. The binding potential of the lead compound was suggested by docking experiments. Interestingly, accurate binding with the VEGFR-2 active pocket was verified through MD simulations (six studies), MM-GBSA (three studies), and DFT (three studies). Additionally, ADMET studies declared the lead compound's drug-likeness. Consequently, the designed lead compound was synthesized and tested for in vitro VEGFR-2 prohibition, cytotoxicity, and safety. Compound **7** exhibited a prohibitory effect against VEGFR-2, with an IC_{50} value of 25 nM (lower than that of sorafenib, 35 nM), besides a promising antiproliferative potential against MCF-7 and HCT 116 cell lines, with very low IC_{50} values of 12.93 and 11.52 µM, as well as high selectivity indexes of 4.32 and 7.28 µM, respectively.

4. Experimental

4.1. In Silico Studies

4.1.1. Docking Studies

Molecular docking was conducted for compound 7 against VEGFR-2 [56,57], using MOE2014 software. A thorough outline has been provided in the Supplementary Data.

4.1.2. MD Simulation

The CHARMM-GUI web server was employed, and GROMACS 2021 was used as an MD engine. A thorough outline has been provided in the Supplementary Data.

4.1.3. MM-GBSA

The Gmx_MMPBSA package was used. A thorough outline has been provided in the Supplementary Data.

4.1.4. DFT

Gaussian 09 and GaussSum3.0 programs were used. A thorough outline has been provided in the Supplementary Data.

4.1.5. ADMET Studies

An ADMET profile was determined using Discovery Studio 4.0 [58,59]. A thorough outline has been provided in the Supplementary Data.

4.1.6. Toxicity Studies

The toxicity profile was determined using Discovery Studio 4.0 [60]. A thorough outline has been provided in the Supplementary Data.

4.2. Chemistry

The solvents and fine chemicals used in the synthesis of the target molecule were purchased from Sigma-Aldrich at a purity above 99%. All chemicals and apparatuses used in this section are illustrated in the Supplementary Data. Compounds **2** and **4** were synthesized according to the previously reported methods [61].

4.2.1. General Procedure for the Synthesis of Compound **5**

To a solution of ester derivative **4** (0.002 mol) in in absolute ethanol (20 mL), hydrazine hydrate 85% (0.01 mol) was added dropwise with continuous stirring. The mixture was heated with gentle reflux for 2 h. After completion of the reaction, the mixture was cooled. The formed precipitate was filtered, dried, and recrystallized from ethanol to give compound **4**.

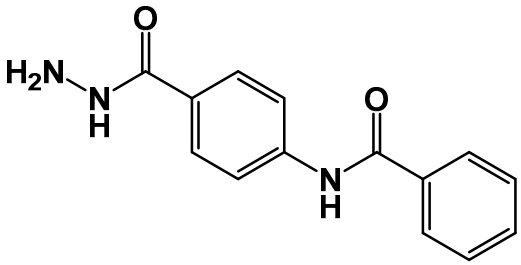

4.2.2. General Procedure for the Synthesis of Compound **7**

To a solution of compound 5 (0.001 mol) in absolute ethanol (50 mL) containing a few drops of glacial acetic acid, (0.001 mol) of 5-methoxy-1*H*-indole-3-carbaldehyde **6** was added. The reaction mixture was heated to reflux for 2 h. The TLC test was used to keep track of the reaction's progress. Under reduced pressure, the solvent was evaporated after

the reaction was completed. The obtained powder was collected and recrystallized from ethanol to furnish the pure form of compound **7**.

(Z)-N-(4-(2-((5-Methoxy-1H-indol-3-yl)methylene)hydrazine-1-carbonyl)phenyl) benzamide.

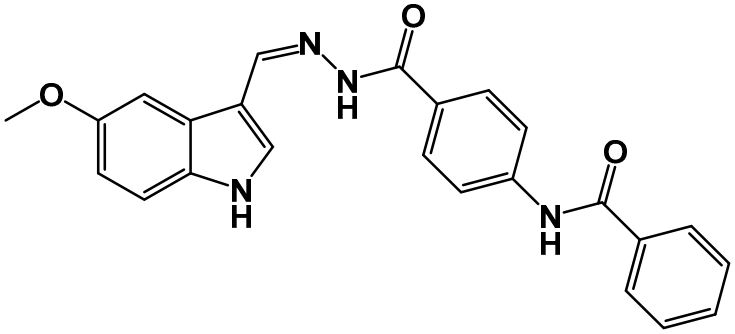

Off-white crystal (yield, 84%); m. p. = 257–259 °C; IR (KBr) ν cm^{-1}: 3287 (NH), 3093 and 3050 (CH aromatic), 2996 and 2956 (CH aliphatic), 1645 (C=O); ^{1}H NMR (400 MHz, DMSO-d6) δ 11.48 (s, 2H), 10.53 (s, 1H), 8.62 (s, 1H), 7.99 (d, J = 8.2,Hz, 2H), 7.96 (m, 4H), 7.88 (d, J = 2.5 Hz, 1H), 7.79 (d, J = 2.4 Hz, 1H), 7.68–7.61 (m, 1H), 7.58 (d, J = 8.2, 2H), 7.36 (d, J = 8.8 Hz, 1H), 6.88 (dd, J = 8.8, 2.4 Hz, 1H), 3.82 (s, 3H); ^{13}C NMR (101 MHz, DMSO-d_6) δ 166.34, 162.36, 154.88, 145.25, 142.42, 135.17, 132.49, 132.31, 131.02, 129.29, 128.95 (2C), 128.67, 128.25 (2C), 125.46, 119.99 (2C), 119.11, 112.90, 112.71, 112.01, 104.67, 55.80, for $C_{24}H_{20}N_4O_3$ (412.45).

4.3. Biological Studies

4.3.1. In Vitro VEGFR-2 Inhibition

Inhibition was performed using a Human VEGFR-2 ELISA kit. A thorough outline has been provided in the Supplementary Data.

4.3.2. In Vitro Antiproliferative Activity

The MTT procedure was employed. A thorough outline has been provided in the Supplementary Data.

4.3.3. Safety Assay

The non-cancerous cell line W138 was used. A thorough outline has been provided in the Supplementary Data.

Supplementary Materials: The detailed methods, spectral data of compound **7** and toxicity report can be downloaded at: https://www.mdpi.com/article/10.3390/pr10071391/s1.

Author Contributions: Conceptualization, A.M.M. and I.H.E.; software, E.B.E., H.E., D.Z.H., I.M.I. and I.H.E.; investigation, R.G.Y. and I.M.M.G.; writing—original draft preparation, A.M.M., H.E. and I.H.E.; writing—review and editing, A.A.A. and E.B.E.; project administration, A.M.M. and I.H.E.; funding acquisition, E.B.E. and A.A.A. All authors have read and agreed to the published version of the manuscript.

Funding: This research was funded by Princess Nourah bint Abdulrahman University Researchers Supporting Project number (PNURSP2022R116), Princess Nourah bint Abdulrahman University, Riyadh, Saudi Arabia. The authors extend their appreciation to the Research Center at AlMaarefa University for funding this work.

Institutional Review Board Statement: Not applicable.

Informed Consent Statement: Not applicable.

Data Availability Statement: Data are available with the corresponding authors upon request.

Conflicts of Interest: The authors declare no conflict of interest.

References

1. WHO Cancer, Fact Sheet. Available online: https://www.who.int/news-room/fact-sheets/detail/cancer (accessed on 13 June 2022).
2. El-Dash, Y.; Elzayat, E.; Abdou, A.M.; Hassan, R.A. Novel thienopyrimidine-aminothiazole hybrids: Design, synthesis, antimicrobial screening, anticancer activity, effects on cell cycle profile, caspase-3 mediated apoptosis and VEGFR-2 inhibition. *Bioorg. Chem.* **2021**, *114*, 105137. [CrossRef] [PubMed]
3. Quesada, A.R.; Muñoz-Chápuli, R.; Medina, M.A. Anti-angiogenic drugs: From bench to clinical trials. *Med. Res. Rev.* **2006**, *26*, 483–530. [CrossRef] [PubMed]
4. El-Zahabi, M.A.; Sakr, H.; El-Adl, K.; Zayed, M.; Abdelraheem, A.S.; Eissa, S.I.; Elkady, H.; Eissa, I.H. Design, synthesis, and biological evaluation of new challenging thalidomide analogs as potential anticancer immunomodulatory agents. *Bioorg. Chem.* **2020**, *104*, 104218. [CrossRef] [PubMed]
5. Alsaif, N.A.; Taghour, M.S.; Alanazi, M.M.; Obaidullah, A.J.; Alanazi, W.A.; Alasmari, A.; Albassam, H.; Dahab, M.A.; Mahdy, H.A. Identification of new [1, 2, 4] triazolo [4, 3-a] quinoxalines as potent VEGFR-2 tyrosine kinase inhibitors: Design, synthesis, anticancer evaluation, and in silico studies. *Bioorg. Med. Chem.* **2021**, *46*, 116384. [CrossRef]
6. Elrazaz, E.Z.; Serya, R.A.; Ismail, N.S.; Albohy, A.; Abou El Ella, D.A.; Abouzid, K.A. Discovery of Potent Thieno [2, 3-d] pyrimidine VEGFR-2 Inhibitors: Design, Synthesis and Enzyme Inhibitory Evaluation Supported by Molecular Dynamics Simulations. *Bioorg. Chem.* **2021**, *113*, 105019. [CrossRef]
7. Sana, S.; Reddy, V.G.; Bhandari, S.; Reddy, T.S.; Tokala, R.; Sakla, A.P.; Bhargava, S.K.; Shankaraiah, N. Exploration of carbamide derived pyrimidine-thioindole conjugates as potential VEGFR-2 inhibitors with anti-angiogenesis effect. *Eur. J. Med. Chem.* **2020**, *200*, 112457. [CrossRef]
8. Cavasotto, C.N.; Aucar, M.G.; Adler, N.S. Computational chemistry in drug lead discovery and design. *Int. J. Quantum Chem.* **2019**, *119*, e25678. [CrossRef]
9. Mahdy, H.A.; Ibrahim, M.K.; Metwaly, A.M.; Belal, A.; Mehany, A.B.; El-Gamal, K.M.; El-Sharkawy, A.; Elhendawy, M.A.; Radwan, M.M.; Elsohly, M.A. Design, synthesis, molecular modeling, in vivo studies and anticancer evaluation of quinazolin-4 (3H)-one derivatives as potential VEGFR-2 inhibitors and apoptosis inducers. *Bioorg. Chem.* **2020**, *94*, 103422. [CrossRef]
10. Eissa, I.H.; El-Helby, A.-G.A.; Mahdy, H.A.; Khalifa, M.M.; Elnagar, H.A.; Mehany, A.B.; Metwaly, A.M.; Elhendawy, M.A.; Radwan, M.M.; ElSohly, M.A. Discovery of new quinazolin-4 (3H)-ones as VEGFR-2 inhibitors: Design, synthesis, and antiproliferative evaluation. *Bioorg. Chem.* **2020**, *105*, 104380. [CrossRef]
11. Eissa, I.H.; Ibrahim, M.K.; Metwaly, A.M.; Belal, A.; Mehany, A.B.; Abdelhady, A.A.; Elhendawy, M.A.; Radwan, M.M.; ElSohly, M.A.; Mahdy, H.A. Design, molecular docking, in vitro, and in vivo studies of new quinazolin-4 (3H)-ones as VEGFR-2 inhibitors with potential activity against hepatocellular carcinoma. *Bioorg. Chem.* **2021**, *107*, 104532. [CrossRef]
12. El-Adl, K.; El-Helby, A.-G.A.; Ayyad, R.R.; Mahdy, H.A.; Khalifa, M.M.; Elnagar, H.A.; Mehany, A.B.; Metwaly, A.M.; Elhendawy, M.A.; Radwan, M.M. Design, synthesis, and anti-proliferative evaluation of new quinazolin-4 (3H)-ones as potential VEGFR-2 inhibitors. *Bioorg. Med. Chem.* **2021**, *29*, 115872. [CrossRef] [PubMed]
13. Yousef, R.G.; Ibrahim, A.; Khalifa, M.M.; Eldehna, W.M.; Gobaara, I.M.; Mehany, A.B.; Elkaeed, E.B.; Alsfouk, A.A.; Metwaly, A.M.; Eissa, I.H. Discovery of new nicotinamides as apoptotic VEGFR-2 inhibitors: Virtual screening, synthesis, anti-proliferative, immunomodulatory, ADMET, toxicity, and molecular dynamic simulation studies. *J. Enzym. Inhib. Med. Chem.* **2022**, *37*, 1389–1403. [CrossRef] [PubMed]
14. El-Helby, A.G.A.; Sakr, H.; Eissa, I.H.; Abulkhair, H.; Al-Karmalawy, A.A.; El-Adl, K. Design, synthesis, molecular docking, and anticancer activity of benzoxazole derivatives as VEGFR-2 inhibitors. *Arch. Der Pharm.* **2019**, *352*, 1900113. [CrossRef] [PubMed]
15. Saleh, N.M.; Abdel-Rahman, A.A.H.; Omar, A.M.; Khalifa, M.M.; El-Adl, K. Pyridine-derived VEGFR-2 inhibitors: Rational design, synthesis, anticancer evaluations, in silico ADMET profile, and molecular docking. *Arch. Der Pharm.* **2021**, *354*, 2100085. [CrossRef]
16. Taghour, M.S.; Elkady, H.; Eldehna, W.M.; El-Deeb, N.M.; Kenawy, A.M.; Elkaeed, E.B.; Alsfouk, A.A.; Alesawy, M.S.; Metwaly, A.M.; Eissa, I.H. Design and synthesis of thiazolidine-2, 4-diones hybrids with 1, 2-dihydroquinolones and 2-oxindoles as potential VEGFR-2 inhibitors: In-vitro anticancer evaluation and in-silico studies. *J. Enzym. Inhib. Med. Chem.* **2022**, *37*, 1903–1917. [CrossRef]
17. Parmar, D.R.; Soni, J.Y.; Guduru, R.; Rayani, R.H.; Kusurkar, R.V.; Vala, A.G.; Talukdar, S.N.; Eissa, I.H.; Metwaly, A.M.; Khalil, A. Discovery of new anticancer thiourea-azetidine hybrids: Design, synthesis, in vitro antiproliferative, SAR, in silico molecular docking against VEGFR-2, ADMET, toxicity, and DFT studies. *Bioorg. Chem.* **2021**, *115*, 105206. [CrossRef]
18. Abdelgawad, M.A.; El-Adl, K.; El-Hddad, S.S.; Elhady, M.M.; Saleh, N.M.; Khalifa, M.M.; Khedr, F.; Alswah, M.; Nayl, A.A.; Ghoneim, M.M. Design, Molecular Docking, Synthesis, Anticancer and Anti-Hyperglycemic Assessments of Thiazolidine-2, 4-diones Bearing Sulfonylthiourea Moieties as Potent VEGFR-2 Inhibitors and PPARγ Agonists. *Pharmaceuticals* **2022**, *15*, 226. [CrossRef]
19. El-Adl, K.; Sakr, H.M.; Yousef, R.G.; Mehany, A.B.; Metwaly, A.M.; Elhendawy, M.A.; Radwan, M.M.; ElSohly, M.A.; Abulkhair, H.S.; Eissa, I.H. Discovery of new quinoxaline-2 (1H)-one-based anticancer agents targeting VEGFR-2 as inhibitors: Design, synthesis, and anti-proliferative evaluation. *Bioorg. Chem.* **2021**, *114*, 105105. [CrossRef]

20. Yousef, R.G.; Sakr, H.M.; Eissa, I.H.; Mehany, A.B.; Metwaly, A.M.; Elhendawy, M.A.; Radwan, M.M.; ElSohly, M.A.; Abulkhair, H.S.; El-Adl, K. New quinoxaline-2 (1 H)-ones as potential VEGFR-2 inhibitors: Design, synthesis, molecular docking, ADMET profile and anti-proliferative evaluations. *New J. Chem.* **2021**, *45*, 16949–16964. [CrossRef]
21. Alanazi, M.M.; Mahdy, H.A.; Alsaif, N.A.; Obaidullah, A.J.; Alkahtani, H.M.; Al-Mehizia, A.A.; Alsubaie, S.M.; Dahab, M.A.; Eissa, I.H. New bis ([1, 2, 4] triazolo)[4, 3-a: 3′, 4′-c] quinoxaline derivatives as VEGFR-2 inhibitors and apoptosis inducers: Design, synthesis, in silico studies, and anticancer evaluation. *Bioorg. Chem.* **2021**, *112*, 104949. [CrossRef]
22. Alanazi, M.M.; Eissa, I.H.; Alsaif, N.A.; Obaidullah, A.J.; Alanazi, W.A.; Alasmari, A.F.; Albassam, H.; Elkady, H.; Elwan, A. Design, synthesis, docking, ADMET studies, and anticancer evaluation of new 3-methylquinoxaline derivatives as VEGFR-2 inhibitors and apoptosis inducers. *J. Enzym. Inhib. Med. Chem.* **2021**, *36*, 1760–1782. [CrossRef]
23. Alanazi, M.M.; Elkady, H.; Alsaif, N.A.; Obaidullah, A.J.; Alanazi, W.A.; Al-Hossaini, A.M.; Alharbi, M.A.; Eissa, I.H.; Dahab, M.A. Discovery of new quinoxaline-based derivatives as anticancer agents and potent VEGFR-2 inhibitors: Design, synthesis, and in silico study. *J. Mol. Struct.* **2021**, *1253*, 132220. [CrossRef]
24. El-Metwally, S.A.; Abou-El-Regal, M.M.; Eissa, I.H.; Mehany, A.B.; Mahdy, H.A.; Elkady, H.; Elwan, A.; Elkaeed, E.B. Discovery of thieno [2, 3-d] pyrimidine-based derivatives as potent VEGFR-2 kinase inhibitors and anti-cancer agents. *Bioorg. Chem.* **2021**, *112*, 104947. [CrossRef] [PubMed]
25. Eissa, I.H.; Alesawy, M.S.; Saleh, A.M.; Elkaeed, E.B.; Alsfouk, B.A.; El-Attar, A.-A.M.; Metwaly, A.M. Ligand and structure-based in silico determination of the most promising SARS-CoV-2 nsp16-nsp10 2′-o-Methyltransferase complex inhibitors among 3009 FDA approved drugs. *Molecules* **2022**, *27*, 2287. [CrossRef] [PubMed]
26. Alsaif, N.A.; Dahab, M.A.; Alanazi, M.M.; Obaidullah, A.J.; Al-Mehizia, A.A.; Alanazi, M.M.; Aldawas, S.; Mahdy, H.A.; Elkady, H. New quinoxaline derivatives as VEGFR-2 inhibitors with anticancer and apoptotic activity: Design, molecular modeling, and synthesis. *Bioorg. Chem.* **2021**, *110*, 104807. [CrossRef] [PubMed]
27. Elkaeed, E.B.; Elkady, H.; Belal, A.; Alsfouk, B.A.; Ibrahim, T.H.; Abdelmoaty, M.; Arafa, R.K.; Metwaly, A.M.; Eissa, I.H. Multi-Phase In Silico Discovery of Potential SARS-CoV-2 RNA-Dependent RNA Polymerase Inhibitors among 3009 Clinical and FDA-Approved Related Drugs. *Processes* **2022**, *10*, 530. [CrossRef]
28. Mohammed, S.O.; El Ashry, E.S.H.; Khalid, A.; Amer, M.R.; Metwaly, A.M.; Eissa, I.H.; Elkaeed, E.B.; Elshobaky, A.; Hafez, E.E. Expression, Purification, and Comparative Inhibition of Helicobacter pylori Urease by Regio-Selectively Alkylated Benzimidazole 2-Thione Derivatives. *Molecules* **2022**, *27*, 865. [CrossRef]
29. Suleimen, Y.M.; Jose, R.A.; Suleimen, R.N.; Arenz, C.; Ishmuratova, M.Y.; Toppet, S.; Dehaen, W.; Alsfouk, B.A.; Elkaeed, E.B.; Eissa, I.H. Jusanin, a New Flavonoid from Artemisia commutata with an In Silico Inhibitory Potential against the SARS-CoV-2 Main Protease. *Molecules* **2022**, *27*, 1636. [CrossRef]
30. Suleimen, Y.M.; Jose, R.A.; Suleimen, R.N.; Ishmuratova, M.Y.; Toppet, S.; Dehaen, W.; Alsfouk, A.A.; Elkaeed, E.B.; Eissa, I.H.; Metwaly, A.M. Isolation and In Silico SARS-CoV-2 Main Protease Inhibition Potential of Jusan Coumarin, a New Dicoumarin from Artemisia glauca. *Molecules* **2022**, *27*, 2281. [CrossRef]
31. Eissa, I.H.; Khalifa, M.M.; Elkaeed, E.B.; Hafez, E.E.; Alsfouk, A.A.; Metwaly, A.M. In silico exploration of potential natural inhibitors against SARS-CoV-2 nsp10. *Molecules* **2021**, *26*, 6151. [CrossRef]
32. Suleimen, Y.M.; Jose, R.A.; Suleimen, R.N.; Arenz, C.; Ishmuratova, M.; Toppet, S.; Dehaen, W.; Alsfouk, A.A.; Elkaeed, E.B.; Eissa, I.H. Isolation and In Silico Anti-SARS-CoV-2 Papain-Like Protease Potentialities of Two Rare 2-Phenoxychromone Derivatives from *Artemisia* spp. *Molecules* **2022**, *27*, 1216. [CrossRef] [PubMed]
33. Alesawy, M.S.; Elkaeed, E.B.; Alsfouk, A.A.; Metwaly, A.M.; Eissa, I. In Silico Screening of Semi-Synthesized Compounds as Potential Inhibitors for SARS-CoV-2 Papain-like Protease: Pharmacophoric Features, Molecular Docking, ADMET, Toxicity and DFT Studies. *Molecules* **2021**, *26*, 6593. [CrossRef]
34. Adnane, L.; Trail, P.A.; Taylor, I.; Wilhelm, S.M. Sorafenib (BAY 43-9006, Nexavar®), a dual-action inhibitor that targets RAF/MEK/ERK pathway in tumor cells and tyrosine kinases VEGFR/PDGFR in tumor vasculature. *Methods Enzymol.* **2006**, *407*, 597–612. [PubMed]
35. Peng, F.-W.; Liu, D.-K.; Zhang, Q.-W.; Xu, Y.-G.; Shi, L. VEGFR-2 inhibitors and the therapeutic applications thereof: A patent review (2012–2016). *Expert Opin. Ther. Pat.* **2017**, *27*, 987–1004. [CrossRef] [PubMed]
36. Pedersen, K.S.; Grierson, P.M.; Picus, J.; Lockhart, A.C.; Roth, B.J.; Liu, J.; Morton, A.; Chan, E.; Huffman, J.; Liang, C. Vorolanib (X-82), an oral anti-VEGFR/PDGFR/CSF1R tyrosine kinase inhibitor, with everolimus in solid tumors: Results of a phase I study. *Investig. New Drugs* **2021**, *39*, 1298–1305. [CrossRef] [PubMed]
37. Rossi, A.; Latiano, T.P.; Parente, P.; Chiarazzo, C.; Limosani, F.; Di Maggio, G.; Maiello, E. The potential role of nintedanib in treating colorectal cancer. *Expert Opin. Pharmacother.* **2017**, *18*, 1153–1162. [CrossRef]
38. Papich, M.G. *Papich Handbook of Veterinary Drugs-E-Book*; Elsevier Health Sciences: Amsterdam, The Netherlands, 2020.
39. El-Helby, A.-G.A.; Ayyad, R.R.; El-Adl, K.; Elkady, H. Phthalazine-1, 4-dione derivatives as non-competitive AMPA receptor antagonists: Design, synthesis, anticonvulsant evaluation, ADMET profile and molecular docking. *Mol. Divers.* **2019**, *23*, 283–298. [CrossRef] [PubMed]
40. El-Helby, A.G.A.; Ayyad, R.R.; Zayed, M.F.; Abulkhair, H.S.; Elkady, H.; El-Adl, K. Design, synthesis, in silico ADMET profile and GABA-A docking of novel phthalazines as potent anticonvulsants. *Arch. Der Pharm.* **2019**, *352*, 1800387. [CrossRef]

41. Wei, K.; Louis, H.; Emori, W.; Idante, P.S.; Agwamba, E.C.; Cheng, C.-R.; Eno, E.A.; Unimuke, T.O. Antispasmodic activity of carnosic acid extracted from rosmarinus officinalis: Isolation, spectroscopic characterization, DFT studies, and in silico molecular docking investigations. *J. Mol. Struct.* **2022**, *1260*, 132795. [CrossRef]
42. Eno, E.A.; Mbonu, J.I.; Louis, H.; Patrick-Inezi, F.S.; Gber, T.E.; Unimuke, T.O.; Okon, E.E.; Benjamin, I.; Offiong, O.E. Antimicrobial activities of 1-phenyl-3-methyl-4-trichloroacetyl-pyrazolone: Experimental, DFT studies, and molecular docking investigation. *J. Indian Chem. Soc.* **2022**, *99*, 100524. [CrossRef]
43. Benjamin, I.; Udoikono, A.D.; Louis, H.; Agwamba, E.C.; Unimuke, T.O.; Owen, A.E.; Adeyinka, A.S. Antimalarial potential of naphthalene-sulfonic acid derivatives: Molecular electronic properties, vibrational assignments, and in-silico molecular docking studies. *J. Mol. Struct.* **2022**, *1264*, 133298. [CrossRef]
44. Asogwa, F.C.; Agwamba, E.C.; Louis, H.; Muozie, M.C.; Benjamin, I.; Gber, T.E.; Mathias, G.E.; Adeyinka, A.S.; Ikeuba, A.I. Structural Benchmarking, Density Functional Theory Simulation, Spectroscopic Investigation and Molecular Docking of N-(1H-pyrrol-2-yl) methylene)-4-methylaniline as Castration-Resistant Prostate Cancer Chemotherapeutic Agent. *Chem. Phys. Impact* **2022**, *5*, 100091. [CrossRef]
45. Louis, H.; Mathias, G.E.; Unimuke, T.O.; Emori, W.; Ling, L.; Owen, A.E.; Adeyinka, A.S.; Ntui, T.N.; Cheng, C.-R. Isolation, characterization, molecular electronic structure investigation, and in-silico modeling of the anti-inflammatory potency of trihydroxystilbene. *J. Mol. Struct.* **2022**, *1266*, 133418. [CrossRef]
46. Udoikono, A.D.; Louis, H.; Eno, E.A.; Agwamba, E.C.; Unimuke, T.O.; Igbalagh, A.T.; Edet, H.O.; Odey, J.O.; Adeyinka, A.S. Reactive azo compounds as a potential chemotherapy drugs in the treatment of malignant glioblastoma (GBM): Experimental and theoretical studies. *J. Photochem. Photobiol.* **2022**, *10*, 100116. [CrossRef]
47. Husein, D.Z.; Hassanien, R.; Khamis, M. Cadmium oxide nanoparticles/graphene composite: Synthesis, theoretical insights into reactivity and adsorption study. *RSC Adv.* **2021**, *11*, 27027–27041. [CrossRef]
48. Wang, T.; Husein, D.Z. Novel synthesis of multicomponent porous nano-hybrid composite, theoretical investigation using DFT and dye adsorption applications: Disposing of waste with waste. *Environ. Sci. Pollut. Res.* **2022**, 1–28. [CrossRef]
49. Turchi, M.; Cai, Q.; Lian, G. An evaluation of in-silico methods for predicting solute partition in multiphase complex fluids–A case study of octanol/water partition coefficient. *Chem. Eng. Sci.* **2019**, *197*, 150–158. [CrossRef]
50. Sullivan, K.M.; Enoch, S.J.; Ezendam, J.; Sewald, K.; Roggen, E.L.; Cochrane, S. An adverse outcome pathway for sensitization of the respiratory tract by low-molecular-weight chemicals: Building evidence to support the utility of in vitro and in silico methods in a regulatory context. *Appl. Vitr. Toxicol.* **2017**, *3*, 213–226. [CrossRef]
51. Altamash, T.; Amhamed, A.; Aparicio, S.; Atilhan, M. Effect of hydrogen bond donors and acceptors on CO_2 absorption by deep eutectic solvents. *Processes* **2020**, *8*, 1533. [CrossRef]
52. Wan, Y.; Tian, Y.; Wang, W.; Gu, S.; Ju, X.; Liu, G. In silico studies of diarylpyridine derivatives as novel HIV-1 NNRTIs using docking-based 3D-QSAR, molecular dynamics, and pharmacophore modeling approaches. *RSC Adv.* **2018**, *8*, 40529–40543. [CrossRef]
53. Escamilla-Gutiérrez, A.; Ribas-Aparicio, R.M.; Córdova-Espinoza, M.G.; Castelán-Vega, J.A. In silico strategies for modeling RNA aptamers and predicting binding sites of their molecular targets. *Nucleosides Nucleotides Nucleic Acids* **2021**, 1–10. [CrossRef] [PubMed]
54. Jain, A.N. Morphological similarity: A 3D molecular similarity method correlated with protein-ligand recognition. *J. Comput.-Aided Mol. Des.* **2000**, *14*, 199–213. [CrossRef] [PubMed]
55. Zhang, H.; Ren, J.-X.; Ma, J.-X.; Ding, L. Development of an in silico prediction model for chemical-induced urinary tract toxicity by using naïve Bayes classifier. *Mol. Divers.* **2019**, *23*, 381–392. [CrossRef] [PubMed]
56. Elkady, H.; Elwan, A.; El-Mahdy, H.A.; Doghish, A.S.; Ismail, A.; Taghour, M.S.; Elkaeed, E.B.; Eissa, I.H.; Dahab, M.A.; Mahdy, H.A. New benzoxazole derivatives as potential VEGFR-2 inhibitors and apoptosis inducers: Design, synthesis, anti-proliferative evaluation, flowcytometric analysis, and in silico studies. *J. Enzym. Inhib. Med. Chem.* **2022**, *37*, 397–410. [CrossRef]
57. Alsaif, N.A.; Taghour, M.S.; Alanazi, M.M.; Obaidullah, A.J.; Al-Mehizia, A.A.; Alanazi, M.M.; Aldawas, S.; Elwan, A.; Elkady, H. Discovery of new VEGFR-2 inhibitors based on bis ([1, 2, 4] triazolo)[4, 3-a: 3′, 4′-c] quinoxaline derivatives as anticancer agents and apoptosis inducers. *J. Enzym. Inhib. Med. Chem.* **2021**, *36*, 1093–1114. [CrossRef]
58. Elkaeed, E.B.; Youssef, F.S.; Eissa, I.H.; Elkady, H.; Alsfouk, A.A.; Ashour, M.L.; El Hassab, M.A.; Abou-Seri, S.M.; Metwaly, A.M. Multi-Step In Silico Discovery of Natural Drugs against COVID-19 Targeting Main Protease. *Int. J. Mol. Sci.* **2022**, *23*, 6912. [CrossRef]
59. Belal, A.; Abdel Gawad, N.M.; Mehany, A.B.; Abourehab, M.A.; Elkady, H.; Al-Karmalawy, A.A.; Ismael, A.S. Design, synthesis and molecular docking of new fused 1 H-pyrroles, pyrrolo [3, 2-d] pyrimidines and pyrrolo [3, 2-e][1, 4] diazepine derivatives as potent EGFR/CDK2 inhibitors. *J. Enzym. Inhib. Med. Chem.* **2022**, *37*, 1884–1902. [CrossRef]
60. NIH Methyl 4-Aminobenzoate. Available online: https://pubchem.ncbi.nlm.nih.gov/compound/12082 (accessed on 1 May 2022).
61. NIH Methyl 4-Benzamidobenzoate. Available online: https://pubchem.ncbi.nlm.nih.gov/compound/727255 (accessed on 1 May 2022).